Hindawi
Journal of Nanomaterials
Volume 2024, Article ID 1073915, 29 pages
https://doi.org/10.1155/2024/1073915

Review Article

Review on Medical Applications of Manganese Oxide (Mn^{2+}, Mn^{3+}, and Mn^{4+}) Magnetic Nanoparticles

Rajesh Kumar Manavalan,[1] **Karolinekersin Enoch**,[2] **Alexey Sergeevich Volegov**,[1] **Gurunathan Angusamy**,[3] **and Sitakumaravel Nallasivam**[3]

[1]*Institute of Natural Sciences and Mathematics, Ural Federal University, Yekaterinburg 620026, Russia*
[2]*Department of Nanotechnology, SRM Institute of Science and Technology, Chennai, Tamil Nadu, India*
[3]*Centre for Advanced Materials, Integrated-Inter-Department of LiWET Communications, Aaivalayam-Dynamic Integrated Research Academy and Corporations (A-DIRAC), Coimbatore 641046, India*

Correspondence should be addressed to Rajesh Kumar Manavalan; r.k.manavalan@urfu.ru

Received 20 September 2023; Revised 23 January 2024; Accepted 2 February 2024; Published 20 February 2024

Academic Editor: Baskaran Rangasamy

Apart from our imagination, the nanotechnology industry is rapidly growing and promises that the substantial changes that will have significant economic and scientific impacts be applicable to a wide range of areas, such as aerospace engineering, nanoelectronics, environmental remediation, and medical healthcare. In the medical field, magnetic materials play vital roles such as magnetic resonance imaging (MRI), hyperthermia, and magnetic drug delivery. Among them, manganese oxide garnered great interest in biomedical applications due to its different oxidation states (Mn^{2+}, Mn^{3+}, and Mn^{4+}). Manganese oxide nanostructures are widely explored for medical applications due to their availability, diverse morphologies, and tunable magnetic properties. In this review, cogent contributions of manganese oxides in medical applications are summarized. The crystalline structure and oxidation states of Mn oxides are highlighted. The synthesis approaches of Mn-based nanoparticles are outlined. The important medical applications of manganese-based nanoparticles like magnetic hyperthermia, MRI, and drug delivery are summarized. This review is conducted to cover the future impact of MnO_x in diagnostic and therapeutic applications.

1. Introduction

Nanoparticles (NPs) have bloomed as a windfall in medical applications, thanks to their exclusive physical and chemical properties [1]. NPs are extensively used in different biomedical applications, such as drug delivery [2], bioimaging [3], hyperthermia [4], cell labeling [5], gene delivery [6], tissue engineering [7], implants [8], antimicrobial agents [9], photothermal therapy [10], immunotherapy [11], and biosensing [12]. The tunable size and shape of the NPs facilitated their usage in therapeutic applications by inflecting the blood circulation, biodistribution, and excretion of the NPs from the body [13]. The quantum efficiency and magnetic properties of the NPs increased their usage in diagnostic applications like fluorescence and magnetic resonance imaging (MRI) [14]. The different NPs used in the medical applications are metal NPs, metal oxide NPs, carbon-based NPs, polymer-based NPs, and magnetic nanoparticles [15]. Metal NPs used in medical applications are silver, gold, platinum, titanium, ceria, palladium, cerium, zinc, copper, etc. [16]. Metal oxide NPs used in medical applications are copper, iron, zinc, titanium, zirconium, and cerium oxide. Carbon-based NPs like graphene, fullerenes, carbon nanotubes, and quantum dots are extensively used in biomedical applications [17]. Among these, magnetic NPs are surging as prominent NPs in various applications like hyperthermia, targeted drug delivery, tissue engineering, theranostic, and lab on a-chip by its magnetic and chemical properties and specificity. A significant boon of employing magnetic nanoparticles in medical applications is that the required magnetic properties of the NPs can be modulated by the external magnetic field [18]. Magnetic NPs are used in various forms pure metals, metal oxides, and metal nanocomposites. The magnetic NPs can be prepared from pure metals Fe, Co, Ni, or a mixture of metals and polymers

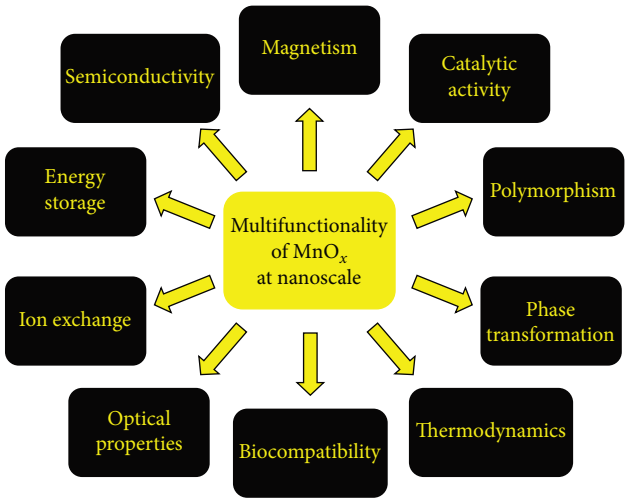

Figure 1: Schematic representation of MnO_x at the nanoscale.

[19]. Generally, iron oxide nanoparticles (Fe_3O_4, γ-Fe_2O_3) are widely used magnetic particles, and the magnetic properties of the IONP can be enhanced by doping with other metals and rare earth metals [20]. Iron oxide nanoparticles doped with gadolinium (Gd) [21], cobalt (Co) [22], zinc (Zn) [23], manganese (Mn) [24], and nickel (Ni) [25] expressed better magnetic properties resulting in the improved contrast effects in MRI that are prominent than bare Fe_3O_4 NPs. Manganese oxides possess good magnetic properties and exist in the several oxides forms of MnO, MnO_2, Mn_2O_3, and Mn_3O_4. The multifunctionality of MnO_x at the nanoscale is represented in Figure 1 [26]. Manganese oxides have been a spotlight in applications like biosensing, bioimaging, drug delivery, and tumor therapy by virtue of their physical and chemical properties, biocompatibility, and tunable structure and morphologies [27]. The medicinal applications of manganese oxide nanomaterials are represented in Figure 2. Manganese oxides also extended their potential in various applications like batteries [28], supercapacitors [29], energy storage systems [30], water purification [31], ion exchange [32], and fertilizer [33]. Besides, manganese is a vital nutrient and plays the role of a cofactor for various enzymes. Mn_xO_y nanoparticles are considered to be safe and showed themselves a suitable candidate T_1 weighted MRI, fluorescent imaging, CT, and theranostic applications [34]. Mn NPs expressed a remarkable T_1 relaxation rate compared to available Gd-based contrast agents [35].

This review endeavors to acquaint the overview of the significant characteristics and crystal structures of manganese oxides and their medicinal applications. This review is categorized into the following sections: The first section covers the crystal structures and synthesis approaches implied for the preparation of manganese oxide nanoparticles. The second portion describes the different oxidation states of Manganese oxides. Finally, we discuss the different medical applications of manganese oxides like hyperthermia, MRI, and drug delivery. This review will certainly contribute to the research to explore much about manganese oxides, especially in the inevitable medical applications.

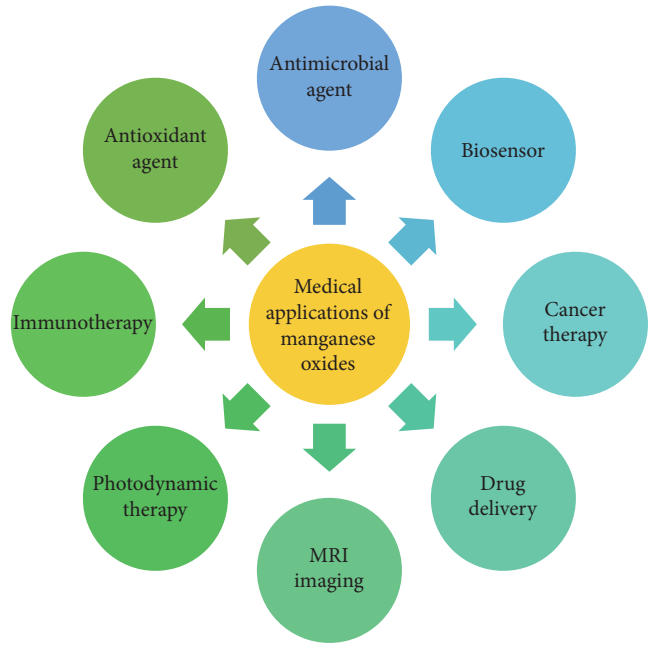

Figure 2: Schematic representations of medical applications of manganese oxides.

2. Manganese Oxides

2.1. Crystal Structures. Manganese is the 10th most bounteous element in Earth's crust. It can be readily oxidized and naturally exhibits 30 different crystalline forms of oxides, hydroxides, and oxyhydroxides that possess a massive number of structural geometries. Generally, manganese oxides are termed MnO_x and the fundamental building block for all the atomic structures of Mn oxide is MnO_6 octahedron [36]. The different atomic structures are formed from the sharing edges or corners in the octahedra. The crystal structures of manganese have been classified as tunnel, layered, spinel, and other structures [37]. A common polymorph of MnO_2 is represented in Figure 3.

2.1.1. Tunnel structures. Tunnel Mn oxides are assembled of single, double, or triple chains of edge-sharing of MnO_6 octahedra and form a tunnel-based framework with a cross-section of square or rectangle as the chains share corners [39]. The larger tunnel structures of Mn oxides are fractionally occupied with water molecules or cations. Some of the tunnel structure-based Mn oxides are pyrolusite MnO_2, ramsdellite MnO_2, nsutite MnO_2, hollandite group (R.8–1.5(Mn(IV), Mn(III))$_8O_{16}$, R = Ba, Pb, K, or Na), romanechite $Ba_{0.66}Mn(IV)_{3.68}Mn(III)_{1.32}O_{10}.1{\cdot}34H_2O$. Pyrolusite MnO_2 is the most stable and abundant polymorph of MnO_2, which is analogous to rutile (TiO_2). In pyrolusite MnO_2, framework structure contained tunnels are formed by sharing the single chains of edge-sharing $Mn(IV)O_6$ octahedra with neighboring chains [40]. The ramsdellite structure consists of double chains of $Mn(IV)O_6$ octahedra, each of which comprises two neighboring single chains connected along their octahedral edges. The double chains, in turn, connect

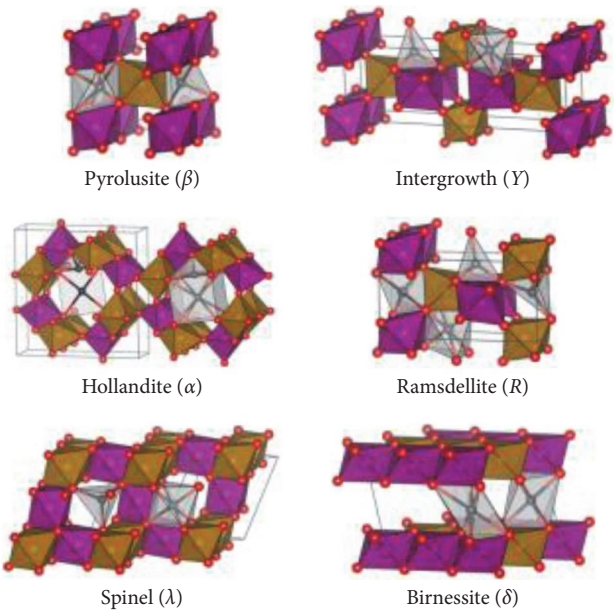

Figure 3: Common polymorphs of MnO_2 (reproduced with permission from [38], JACS, 2017).

corners to create a structure with tunnels with 1×2 octahedral cross-sections on each side [41]. Nsutite MnO_2, also known as gamma MnO_2, owns an improper crystal lattice. Nsutite structures are found to be the ordered intergrowths of ramsdellite and pyrolusite. Double chains of edge-sharing MnO_6 octahedra form the hollandite structure; however, they are joined together to create tunnels with square cross-sections that are two octahedra on a side. In romanechite structures, tunnel structures are formed as rectangular cross-sections by the linkage of double and triple chains of edge-sharing MnO_6 octahedra. One of the main Mn minerals found in ocean Mn nodules is todorokite, the most likely host phase for essential metals like Ni, Co, etc. It is a significant mineral having zeolite-like tunnel structures [42, 43].

The tunnel-based structure is also present in the MnOOH minerals and their polymorphs. Manganite is the most stable and typical of the three naturally occurring polymorphs of MnOOH; the other two are feitknechtite and groutite. The crystal structure of manganite (γ-MnOOH) is comparable to that of pyrolusite, except all of the Mn is trivalent, and half of the O atoms are swapped out for hydroxyl anions. The hydroxyl anions in groutite (α-MnOOH) have completely replaced all of the Mn(III) and half of the O anions, much like in manganite. Naturally existing (β-MnOOH) is said to be feitknechtite [44].

2.1.2. Layered Structure. The layered structure-based Mn oxide are lithiophorite $LiAl_2(Mn(IV)_2Mn(III))O_6(OH)_6$, chalcophanite $ZnMn_3O_7{\cdot}3H_2O$, birnessite group (Na, Ca,Mn(II)) $Mn_7O_{14}2{\cdot}8H_2O$ [45]. The lithiophorite structure comprises a stack of MnO_6 sheets alternated with $Al(OH)_6$ octahedra sheets, where one-third of the octahedral sites are vacant. Li cations occupy the vacant sites in the Al layer, and the charge is balanced by replacing an equal number of Mn(III) for Mn(IV) cations. The layers are framed by the H-bond crosslinking between the hydroxyl of the Al/Li layer and the O atoms of the Mn sheet. Chalcophanite $ZnMn_3O_7{\cdot}3H_2O$ structure holds edge-sharing $Mn(IV)O_6$ octahedra with the alternating layer of Zn cations and water molecules. The Zn cations are located above and below the unoccupied octahedral site in the Mn layer, where one-seventh of the octahedral site is unoccupied. The basic structure of the birnessite group is a MnO_6 octahedra sheet where the interlayer cations and water molecules occupy different positions and possess dominant interlayer cations between Ca and Mn(II) [42, 46].

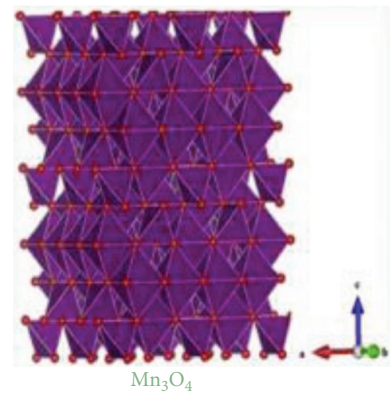

Figure 4: Hausmmanite structure of Mn_3O_4 (reproduced with permission from [49], Elsevier, 2020).

Another layered structure of MnO_2 is vernadite $MnO_2{\cdot}nH_2O$, a fine grained, poorly crystalline natural Mn oxide phase. Vernadite is a variety of birnessite that is disordered in the layer-stacking direction [47].

2.1.3. Spinel Structure. Hausmannite ($Mn(II)Mn(III)_2O_4$) has a spinel-like structure with Mn(II) in the tetrahedral and Mn(III) in the octahedral sites. Mn_3O_4 unit cell comprises 32 oxygen and 24 cations of both Mn^{2+} and Mn^{3+} [48]. The spinel structure of Mn_3O_4 is shown in Figure 4.

2.2. Methods of Synthesis of Nanoparticles. Generally, nanoparticles are prepared using broadly categorized approaches like top-down and bottom-up. In top-down approaches, the nanoparticles are fabricated by decomposing larger molecules into smaller molecules. Several examples of top-down approaches include lithographic techniques, chemical vapor deposition, physical vapor deposition, ball milling, etc. In the bottom-up approach, the nanoparticles are prepared using assembling nanostructures from smaller components like atoms or molecules. The synthesis method follows bottom-up approaches sol–gel, hydrothermal, green synthesis, and biochemical synthesis. The size, shape, morphology, stability, and scalability of the nanoparticles rely on the synthesis methods. The different approaches like physical, chemical, and biosynthesis for the synthesis of MnO_x-based nanoparticles are discussed in this section.

2.2.1. Chemical Approach.

(1) Hydrothermal Method. The hydrothermal method is the extensively employed synthesis route for the preparation of Mn oxide nanoparticles, exploits the different reaction vessel known as Teflon lined autoclave to perform the hydrothermal

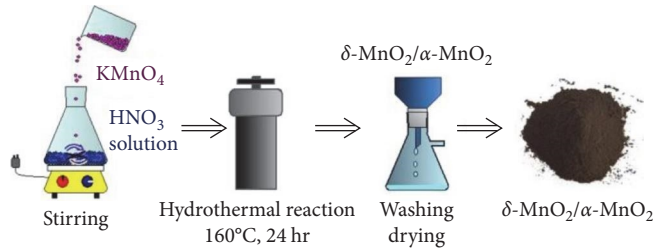

Figure 5: Schematic representation of hydrothermal synthesis of α-MnO_2 and δ-MnO_2 (reprinted with permission from [54], Springer, 2022).

reaction which favors the solubility and reactivity in high-pressure environment [50]. Hydrothermal synthesis can be employed in a wide range of temperatures from room temperature to high temperature. The controlled morphology can be obtained by performing the reactions in low- or high-pressure conditions based on the vapor pressure of the composition involved in the reaction [51]. The particle aggregation and size of the nanoparticle are controlled by using surfactants like CTAB and gelatin. The morphology and the crystal structure can be tuned by the molar composition of the precursor and the solvent involved in the reaction. Wang and Li [52] reported the preparation of α and β phases of MnO_2 by varying the concentration of the ammonium and sulfate ions in the reaction between ammonium persulphate and magnesium sulfate. Duan et al. [53] prepared MnO_2 nanostructures with different crystal phases (α-, β-, and γ-MnO_2) using $KMnO_4$ using the hydrothermal method. The different morphologies like nanorod, nanoflower, nanowall, nanosheet, and nanowire were obtained by optimizing the reaction temperature and concentration of $KMnO_4$. Arkhipova et al. [54] also reported the concentration of the precursor plays an important role in obtaining different crystal structures. α-MnO_2 was prepared using 1.98 g of $KMnO_4$ and δ-MnO_2 using 3.96 g, the excess K^+ ion was required to stabilize the δ-MnO_2. The schematic representation of hydrothermal synthesis is represented in Figure 5. Wang et al. [55] prepared α-MnO_2, γ-MnOOH, and Mn_3O_4 nanomaterials using manganese acetate and NaOH at 180°C for different duration of 3, 11, and 24 hr. Needle-shaped manganese oxide nanoparticle having high surface area and porous structure was prepared via one-step hydrothermal approach using $KMnO_4$ and H_2SO_4 [56]. Furthermore, the temperature involved in the hydrothermal reactions determines the crystal structure and influences the process of crystal growth, higher crystallinity is attained by increasing the reaction temperature. Cao et al. [57] reported the change in α-MnO_2 to β-MnO_2 as the temperature increases from 160 to 200°C, as shown in Figure 6. Hashemzadeh et al. [58] reported the comparison of manganese oxides prepared by hydrothermal and sol–gel methods. It is observed that the diameter of nanorods synthesized by the hydrothermal method was found to be around 50–100 which was smaller than the nanorods prepared by the sol–gel method.

Hydrothermal reactions are also employed for the synthesis of manganese oxide-based composites like Nd_2O_3/Mn_3O_4 [59], MnO_2/graphene [60], Sn@rGO-MnO_2 [61], and MnO_2/NiO@Ni [62].

(2) Sol–Gel. Sol–gel is a facile method employed to form refined and pure crystal structures with uniform morphology by controlling the reaction at the molecular level. This method is more favorable for the preparation of thickness-controlled film. Hydrolysis and condensation are the two important processes involved in this sol–gel method. The inorganic precursors are hydrolyzed with water, acid, alcohol, or base and condensed to form a 3D molecular network. The following reactions are involved.

Hydrolysis:

$$M(\mathrm{OR})_4 + \mathrm{H_2O} \longrightarrow \mathrm{HO} - M(\mathrm{OR})_3 + \mathrm{ROH} \longrightarrow M(\mathrm{OH})_4 + 4\mathrm{ROH}. \quad (1)$$

Condensation:

$$(\mathrm{OR})_3\mathrm{M} - \mathrm{OH} + \mathrm{HO} - \mathrm{M}(\mathrm{OR})_3 \longrightarrow (\mathrm{RO})_3\mathrm{M} - \mathrm{O} - \mathrm{M}(\mathrm{OR})_3 + \mathrm{H_2O}, \quad (2)$$

$$(\mathrm{OR})_3\mathrm{M} - \mathrm{OH} + \mathrm{RO} - \mathrm{M}(\mathrm{OR})_3 \longrightarrow (\mathrm{OR})_3\mathrm{M} - \mathrm{O} - \mathrm{M}(\mathrm{OR})_3 + \mathrm{ROH}, \quad (3)$$

where M refers to the Metal and R is the alkyl group.

Initially, the precursor is dissolved in the solvent to form a homogenous solution. Then, stable sols are formed from the agglomerates due to the interaction of solute and solvent or interaction between the solute. After evaporation sols are converted into gels, and oxides are formed followed by the sintering of gels at a required temperature. The reaction involved in the sol–gel method can be optimized by the different parameters like temperature, pH, reaction time, and concentration of the solution. Birnessite manganese dioxide of lamellar type was produced from mixed oxides, A-MnO ($A = K^+$, Na^+) by sol–gel route. The manganese oxides are formed from the reduction of aqueous permanganate solutions using organic reducing agents followed by drying and calcination. The ternary oxides are formed by the reaction of alkaline cations (K^+ and Na^+) with manganese oxides [63]. Siddique et al. [64] prepared manganese oxide nanoparticles using the redox reaction of glycerol and potassium, calcined at two different temperatures at 400–700°C. The surface morphology of the MnO_2 calcined at 700°C shows less aggregation than 400°C. Yarbrough et al. [65] reported the effect of solvent and concentration of precursor on the morphology of Mn_3O_4 nanoparticles. The Mn_3O_4 nanoparticles were formed by the hydrolysis and condensation of manganese acetate in the presence of

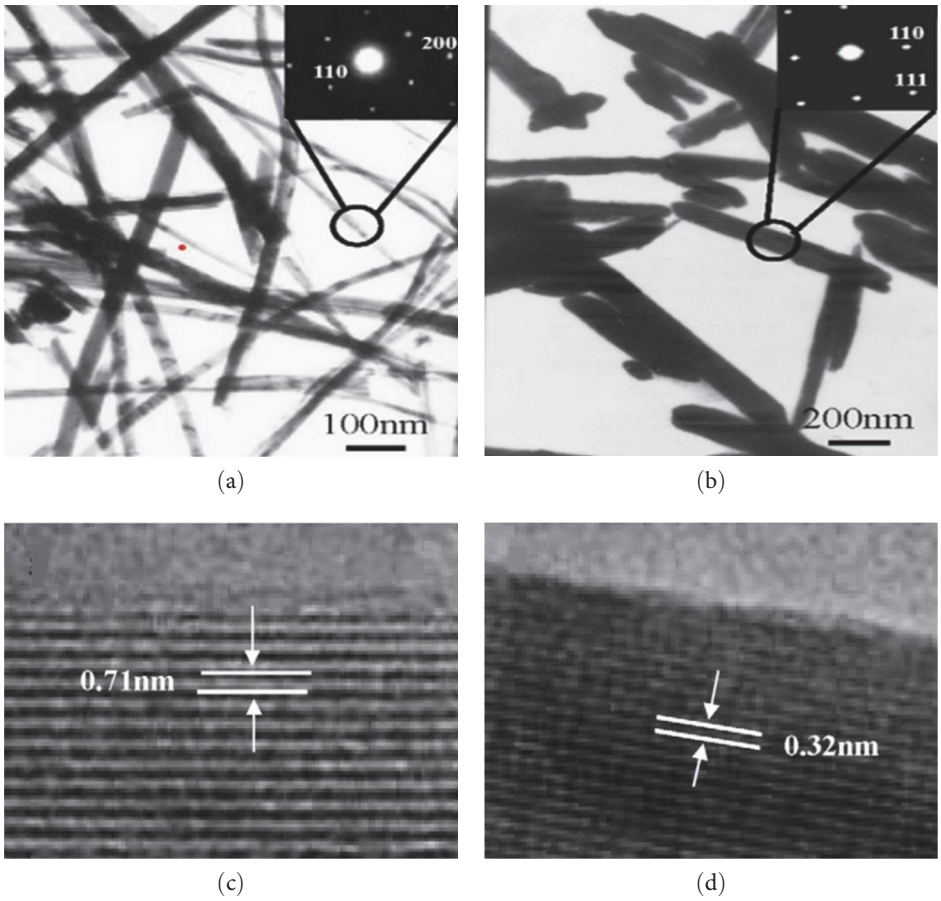

Figure 6: (a, b) TEM images of α-MnO_2 and β-MnO_2 at 160 and 200°C; (c, d) HR TEM images of α-MnO_2 and β-MnO_2 at 160 and 200°C (reprinted with permission from [57], Elsevier, 2010).

sodium hydroxide in three different solvents water, 70% ethanol, DMF, and toluene. It is reported that the Mn_3O_4 NPs prepared using the solvent water, ethanol, and toluene yielded hexagonal structures, whereas DMF resulted in irregular nanoparticles. The average diameter of the Mn_3O_4 NPs ranged from 100 to 200 nm for the solvent water, ethanol, and toluene irrespective of the different molar concentrations. Though the sol–gel approach is a facile technique possibility of agglomeration is more [66].

(3) Electrochemical Synthesis. The electrochemical synthesis method is an inexpensive technique widely used for the deposition of metal and metal oxide. The morphologies of the deposited materials can be optimized by the different parameters like bath composition, temperature, and current. This method results in the deposition of highly pure material on a conducting substrate, i.e., stainless steel, graphite, titanium, etc. The reactions involved in the electrodeposition of manganese oxide nanoparticles are as follows:

$$Mn^{2+} + 2H_2O \longrightarrow MnO_2 + 2e^{-1}. \quad (4)$$

Electrochemical deposition of manganese oxide nanoparticles prepared from different precursors like manganese acetate, manganese chloride, manganese sulfate, etc. The structure, surface area, and oxidation state of the manganese nanoparticles depend on the deposition potential and conditions. The working electrode utilized for the deposition of material must be cleaned with nitric acid and water and blow dried in the steam of nitrogen for the pure deposition. Lee et al. [67] reported the anodically electrodeposited manganese oxide nanoparticles using manganese acetate aqueous solution in a three-cell system consisting of a platinum plate, gold plate, and Ag/Agcl at three different modes, constant potential (CP) at 1 V for 900 s, pulse potential (PP) at 1 and 0 V with 0.5/0.5 s on–off time for 10,000 s, and pulse reverse potential (PRP) at 1 and 1 V with 0.5/0.5 s interval time for 10,000 s. It is reported that the morphology of the manganese oxide nanostructures varies according to the pattern of applied potential, traditional bulk film composed of a large agglomerate particle was obtained in CP mode, flower petal shaped MnO_x particles were obtained in PP mode, more defined nanostructure was obtained in PRP mode. Li and Park [68] reported that the coating of manganese oxides over vertically aligned carbon nanotubes by the depositing the aqueous mixture of 0.1 M Na_2SO_4 and 0.02 M $MnSO_4$. It is stated that the 5 mA of deposition current was utilized for the high nucleation density without anodic oxygen evolution. Nakayama et al. [69] reported the electrodeposition of layered manganese oxide nanocomposites by applying 1.0 V with a charge of 330 mC/cm^2. Broughton and Brett [70]

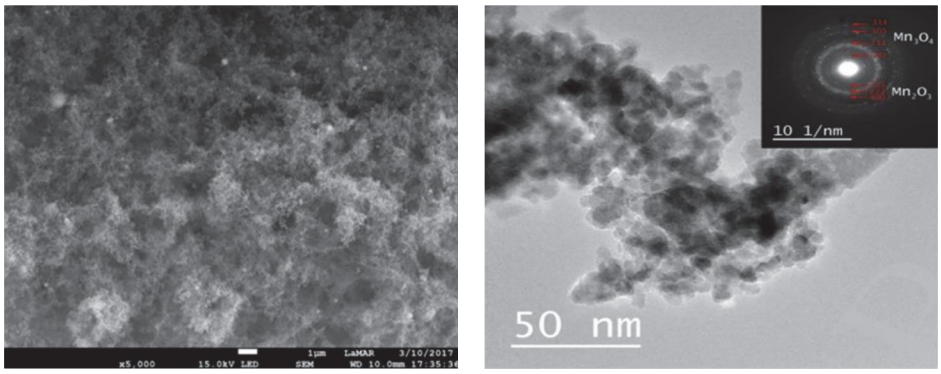

(a) (b)

Figure 7: (a) Low magnification and cross-section SEM image of Mn foam; (b) high resolution TEM images (reprinted with permission from [77], Elsevier, 2019).

demonstrated the efficiency of the deposition of MnO_2 relays on both anions and cations. It is reported that the acetate ion expressed the controllable effect on the deposition potential of MnO_2 produced from the mixture of manganese sulfate- and acetate-based electrolyte. Acetate ions also reduce the reduction potential required for the eletrodeposition [70].

(4) Precipitation Method. The chemical precipitation method is a simple, inexpensive technique used in the synthesis of various nanomaterials at low temperatures. The formation of nanoparticles by precipitation method depends on the different parameters like pH, reaction temperature, and concentration of the reacting precursor. Kanha and Saengkwamsawang [71] prepared α-MnO_2 nanostructures using $KMnO_4$ and Tris (2-hydroxyethyl)amine in different stirring times (0.5, 1, 2, and 3 hr). The results indicated that the crystallite size and strain of α-MnO_2 is less as the stirring time is increased and the increase in calcination duration resulted in the increase in particle size. Chen et al. [72] reported the shape-controlled synthesis of 1D MnO_2 of different crystallographic forms and morphologies using $MnCl_2{\cdot}4H_2O$ and $KMnO_4$. It is observed that the ratio of DI water/Isopropanol and the concentration of $KMnO_4$ play an important role in morphology. The ratio of DI water/Isopropanol contributes to the structural differences of the intermediate species for crystal growth owing to the discrepant coordinate abilities between DI-water and isopropanol with MnO_6 octahedron units and the concentration of $KMnO_4$ inducing the stacking behavior of the nuclei during the crystal growth period. Wang et al. [73] reported the preparation of different crystallographic phases γ-MnO_2, Mn_2O_3, and Mn_3O_4 at different calcination temperatures. Some of the manganese-based nanocomposites prepared using the coprecipitation method are MnO_x–CeO_2 [74], MnO_x–ZrO_2 [75], and Fe–Mn [76]. Thus, the size and morphology of nanoparticles prepared using coprecipitation method rely on the different reaction parameters like concentration of the precursor, ratio, and proportion of the solvent, temperature, stirring duration, calcination temperature, and duration.

2.2.2. Physical Approach. In the physical approach, pulsed laser deposition was employed to prepare specific nanomaterials with controlled size using the high power density laser with narrow frequency. Initially, the manganese target material is heated in a vacuum by the pulsed laser to melt and ablate the surface. Then the atoms ablated or vaporized from the surface of the target deposited on the substrate. Lacerda et al. [77] reported the preparation of manganese oxide nanofoam from a metallic Mn target in a 5 Torr pressure O_2 buffer atmosphere. The Mn metallic target ablation was attained by the Nd:YAG laser of 1,064 nm wavelength, pulse duration of 7 ns, and 10 Hz repetition rate. The morphological analysis of the Mn Nanofoam obtained by SEM and TEM is represented in Figure 7. Corrales et al. [78] reported the preparation of MnO_2 nanoparticles by Nd: YAG laser of 1,064 nm, 9 ns, and 10 Hz from the target MnO_2. Xia et al. [79] reported the manganese oxide thin film of different oxidation states from a metallic Mn target using an excimer laser of 240 nm, laser fluence of 2 Jcm^{-2}, and repetition rate of 10 Hz. The chamber was evacuated below the pressure of 10^{-5} Torr before the deposition followed by the introduction of high-purity oxygen and thin film was deposited at 600°C. The different oxidation states of manganese oxides are obtained by varying the partial oxygen pressures from 0 to 700 mTorr. XRD patterns revealed that the face-centered cubic phase of MnO in the no oxygen atmosphere, a pure tetragonal hausmannite Mn_3O_4 phase is obtained at 200 mTorr, as the oxygen content increased to 700 mTorr, a pure orthorhombic Mn_2O_3 phase is obtained. The different phase composition of the manganese oxides can be attained by varying the oxygen partial pressure. The morphology of the manganese oxide film at different oxygen partial pressure is represented in Figure 8. The different oxidation states of the manganese oxides can be obtained by changing the substrate temperature. Isber et al. [80] reported that the Mn_2O_3 phase is obtained until the temperature of 700°C and phase transformation of Mn_3O_4 occurred above the temperature of 700°C. The structure and phase of the nanoparticle can be varied with the temperature of the substrate, oxygen partial pressure, metallic target, deposition duration, and wavelength of the laser.

Another physical approach adapted for the synthesis of MnO_x nanoparticles is ball milling. Ochirkhuyag et al. [81] reported that the MnO_x nanostructures are prepared by milling $MnCl_2{\cdot}4H_2O$ and $KMnO_4$ with 0.09 M of sodium hydroxide and 5 mL of water using stainless grinding balls. It is also worth mentioning that the milling speed could tailor the crystal structure and the oxidation states of the

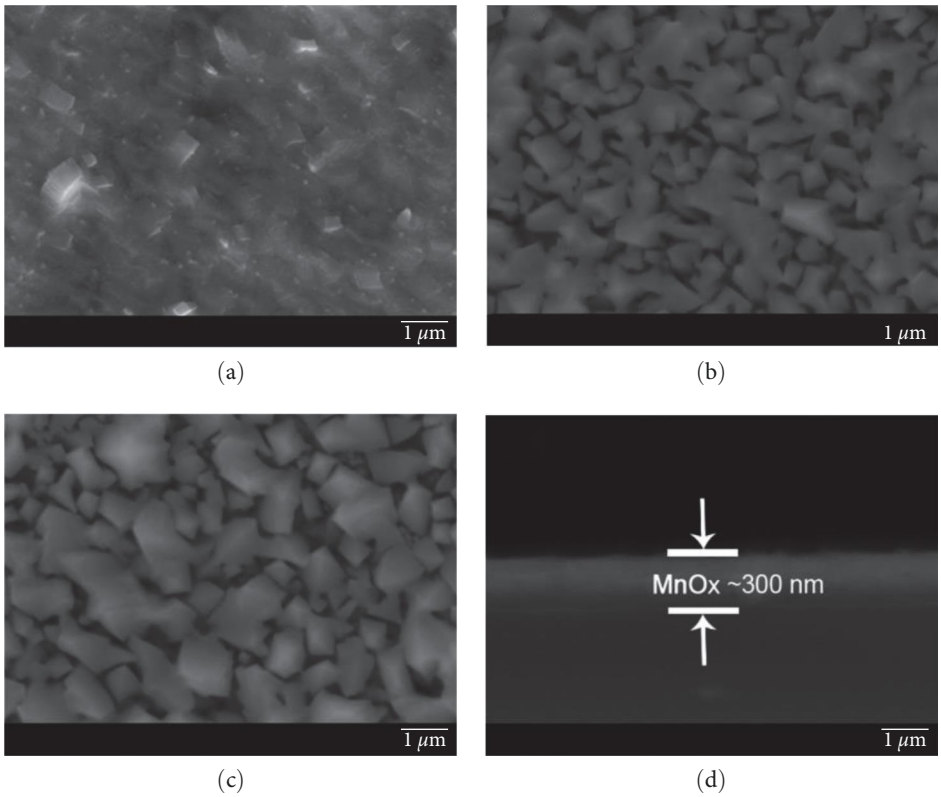

Figure 8: FESEM images of (a) the MnO thin film, (b) the Mn_3O_4 thin film, (c) the Mn_2O_3 thin film, and (d) cross-section FESEM image of a Mn_3O_4 thin film deposited on a Si substrate (reprinted with permission from [79] Elsevier, 2009).

manganese. Villanueva et al. [82] reported that the manganese oxide perovskite for the hyperthermia was synthesized by milling in an agitate mill and fired at 1,400°C. In some cases, microwave-assisted ball milling was used to prepare Mn-based ferrites. There are several factors like milling duration and speed, ball-to-powder weight ratio, and type of milling balls and containers influence the shape, size, and structure of the MnO_x-based nanoparticles [83].

(1) Biogenic Synthesis. Biogenic synthesis involves the synthesis of nanoparticles using microorganisms or plant extract. This approach is a boon to the nanotechnology, thanks to its features like environmentally friendly, nontoxic, and less expensive. The preparation of manganese NPs using plant extract is based on the reduction and stabilization of manganese metal into Mn NPs. The phytochemicals of plant extracts like alkaloids, flavonoids, phenolic, and terpenoids are involved in the process of reduction and also act as a capping agent to control the size of the nanoparticles. In many cases, size and shape of the nanoparticles are controlled using the extract and the amount of phytochemicals involved in the reduction of metal ions matters for the optimization of the size of the nanoparticles.

Khan et al. [84] reported the preparation of MnO NPs of ~85 nm using the leaf extract of *Abutilon indicum* leaf extract. The phytomolecules like flavonoids, phenolics, and carbohydrates present in the *A. indicum* leaf extract reduced the Mn^+ into their zero valent species Mn^0 by donating electrons through a redox reaction and other phytomolecules like alkaloids, proteins, etc., contributed in the stabilization of Mn^0. The mechanism of formation of MnO NPs involved the reduction of Mn^+ into their zero valent species. FTIR results of the *A. indicum* leaf extract and MnO nanoparticles endorsed that the phytomolecules present in the extract were involved in the reduction of Mn ions and stabilization of Mn NPs. The schematic representation of the preparation of MnO NPs using *A. indicum* leaf extract is represented in Figure 9. Souri et al. [85] reported that an increase in the concentration of extract prepared from the aerial parts of *Dittrichia graveolens* resulted in an increased synthesis rate in the production of MnO. MnO_2 NPs were prepared using the leaf extract of *Viola betonicifolia* expressed better antioxidant, antimicrobial, and cytotoxic effects than the pure leaf extract. Also, the physical characterization revealed that highly crystalline, spherically shaped, homogeneously dispersed MnO_2 NPs were obtained with a particle size of 10.5 $\pm$ 0.85 nm [86]. The physical characterization of MnO_2 NPs synthesized using *V. betonicifolia* is represented in Figure 10. Prasad and Patra [87] reported the synthesis of MnO_2 nanorods in the diameter of 100–200 nm using phyllanthus amarus as a reducing agent and curcumin as a stabilizing agent. Several studies reported the preparation of MnO_2 nanoparticles using various extracts like *Caryota mitis Lour*. (Fishtail palm) flower [88], *Leucaena Leucocephala* [89], and green tea [90]. Diallo et al. [91] prepared Mn_3O_4 NPs in the diameter of 18–28 nm by *Aspalathus linearis* extract using the precursor, manganese chloride. The formation mechanism of Mn_3O_4

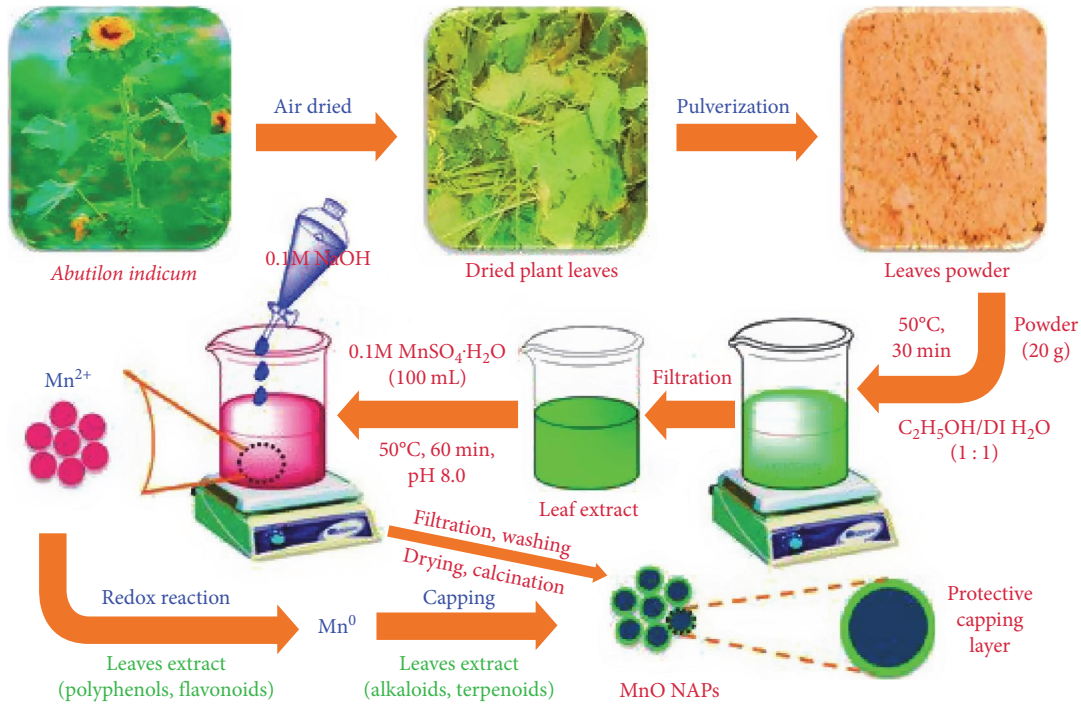

FIGURE 9: Schematic representation of preparation of MnO NPs using *A. indicum* leaf extract (reprinted with permission from [84], MDPI, 2020).

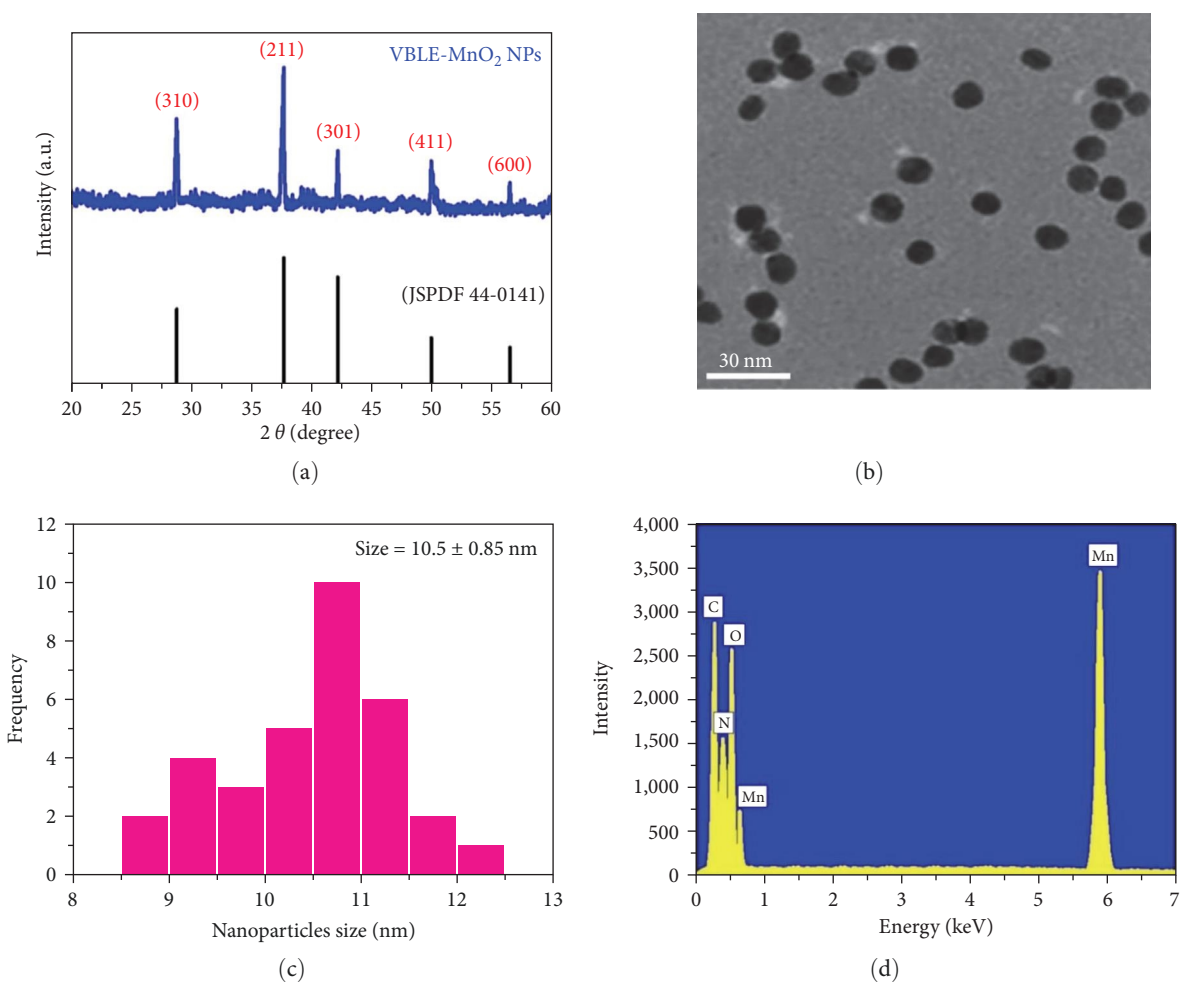

FIGURE 10: (a) XRD pattern, (b) TEM image, (c) size distribution, and (d) EDX pattern for the green synthesized MnO_2 NPs using *V. betonicifolia* (reprinted with permission from [86], Frontiers, 2021).

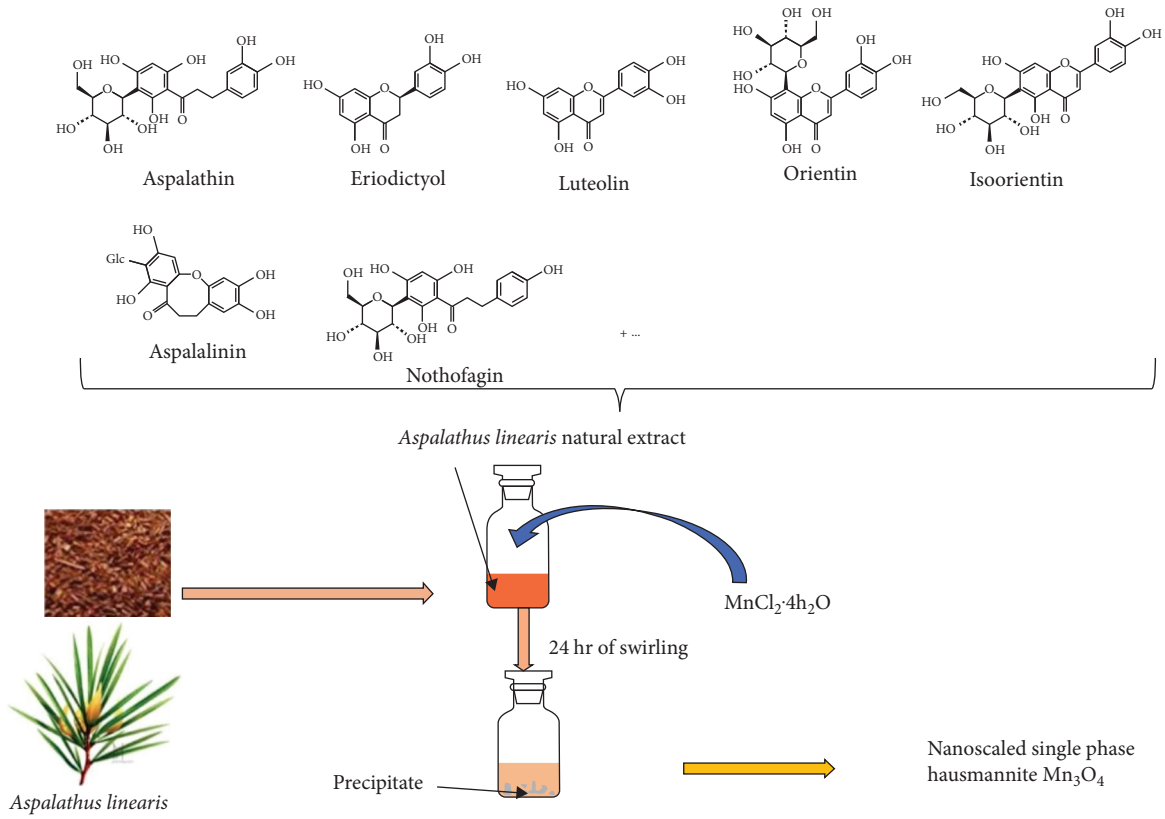

FIGURE 11: Schematic representation of formation of Mn_3O_4 NPs using *Aspalathus linearis* extract (reprinted with permission from [91], Springer, 2021).

NPs using *A. linearis* extract is represented in Figure 11. Several studies have reported the formation of Mn_3O_4 using various extracts prepared from *Costus woodsonii* flower [92], *Adalodakam* [93], *Ananas comosus* (L.) peel [94], *Azadirachta indica* [95], *Simarouba Glauca* leaf [96], Green gram powder [97], etc. Premakumari et al. [98] reported the synthesis of dimanganese trioxide nanoparticles, Mn_2O_3 using different concentrations of (0.1, 0.2, and 0.3 g) tamarind seed powder. In the preparation of manganese oxide nanoparticles, the concentration of extract: precursor ratio, temperature, and time play an effective role than pH [99]. Apart from the plant extract, microorganisms also expressed high potential in the preparation of Mn NPs. Microorganisms like yeast, bacteria, and fungi are employed in the synthesis of NPs. The reductase enzymes present in microorganisms are responsible for the reduction of Mn salts into Mn NPs with a limited size distribution. Sinha et al. [100] reported the synthesis of orthorhombic MnO_2 NPs by *Bacillus* sp. cells. In another study, the preparation of Mn_2O_3 by isolated aerobic bacterium from Persian Gulf water for the first time. The acinetobacter bacteria was grown aerobically in K medium along with $MnCl_2$ at 28°C for 14 days followed by the centrifugation of Mn oxide suspension [101]. Salunke et al. [102] reported the synthesis of MnO_2 NPs using the marine bacterium *Saccharophagus degradans* and yeast *Saccharomyces cerevisiae* as a reducing agent for the precursor of potassium permanganate. It is reported that the rapid reduction of $KMnO_4$ solution was accomplished by the supernatant of 96-hr-old *S. cerevisiae* culture broth and yeast extract. Some of the recently prepared various Mn-based oxides and their properties are presented in Table 1.

The synthesis approaches of the nanoparticles substantially affect the efficacy of nanoparticles in biomedical applications. The different properties like size, surface area, stability, and surface functionalization required for the medical applications rely on the synthesis approaches, precursors, and parameters involved in the synthesis. The optimization of surface area and size of the nanoparticles mostly rely on the synthesis and the parameters which are highly imperative to be used in both diagnostic and therapeutic effects as the smaller nanoparticles often exhibit enhanced cellular uptake and can penetrate tissues more effectively [115, 116]. The stability of the nanoparticles is essential to increase the stable performance and prolonged circulation without aggregation and which can be controlled by the synthesis [117]. The biocompatibility of the nanomaterial is a great concern to be used in medical applications and hence suitable approaches and chemicals should be used to enhance the biocompatibility and the functionalization of the surface of the nanoparticles will improve the biocompatibility and its performance resulting in efficient therapeutic and diagnostic effect [118].

3. Manganese—Different (Mn^{2+}, Mn^{3+}, and Mn^{4+}) Oxidation States

Manganese, a transition metal that subsists in different oxidation states includes +2, +3, +4, +6, and +7.

Table 1: Synthesis of various manganese nanoparticles and their properties.

S. no.	Material	Method	Precursor	Temperature (°C)	Size (nm)	Shape	References
1	α-, β-, γ-, and δ- MnO_2 single crystal nanowires/nanorods	Liquid-phase oxidation method	$MnSO_4{\cdot}H_2O$, $(NH_4)_2S_2O_8$, $KMnO_4$	120–180	5 ± 20 and 40 ± 100	Ribbonlike nanowires	[52]
2	α-MnO_2 and δ-MnO_2	Hydrothermal treatment	$KMnO_4$, HNO_3	70	35–50	Nanoneedle structure	[54]
3	α-MnO_2, γ-MnOOH, and Mn_3O_4	Hydrothermal	—	60	~500	Nanoflower-like	[55]
4	α-MnO_2	Simple hydrothermal	$KMnO_4$	60	100–1,000	Long needle-like shape	[56]
5	Nd_2O_3/Mn_3O_4 nanocomposites	Sol–gel method	$MnSO_4{\cdot}H_2O$ and $KMnO_4$	900	30–400	Spherical	[59]
6	MnO_2/reduced graphene oxide (rGO)	Hydrothermal	$KMnO_4$	−40	0.21−0.22	Birnessite-type	[60]
7	MnO_2, MnO_4, MnO_7	Gel formation process	$KMnO_4$	400–700	32.7, 28.3	Spherical	[64]
8	Manganese oxide	Pulse reverse electrodeposition technique	Manganese acetate	—	~400 nm	Flower petals	[67]
9	MnO_2/VACNTs	Pulsed current electrodeposition method	—	50	~500	Spherical	[68]
10	MnO_2	Coprecipitation method	$KMnO_4$	400	20–80	Tetragonal	[71]
11	Manganese oxide nanofoam	Pulsed laser deposition	—	300, 400, 500	10	Foam like	[77]
12	MnO_2	Laser ablation method	—	—	90–160	Spherical shape	[78]
13	MnO_2	Cyclic voltammetry method	$Mn(CH_3COO)_2$ and Na_2SO_4	60	0.21–0.26	Short staggered nanorod shape	[103]
14	MnO_2 films	Electrochemical deposition method	$Mn(CH_3COO)_2$ and Na_2SO_4	60	20–50 nm in diameter	Spherical	[104]
15	Manganese oxide (α-MnO_2) nanoparticles	Chemical precipitation method	Manganese chloride, $KMnO_4$	500	41.49	Spherical	[105]
16	γ-MnO_2 (Nsutite) nanoparticles	Sol–gel technique	—	100	—	Rice-like morphology	[106]
17	δ-MnO_2 nanosheet array	One-step electrodeposition	—	—	—	Nanosheet structures	[107]
18	MnO nanoparticles cobalt–manganese oxide	Chemical precipitation technique	manganese chloride ($MnCl_2$) and sodium hydroxide (NaOH)	500	28	Spherical shape	[108]
19	Serotonin−stearic acid (ST-SA)/ manganese oxide nanocuboids (MNCs)	Chemical precipitation method	—	80	~18 and ~21	Cuboid shape	[109]
20	MnO_2/silver (Ag) nanoparticles	Sol–gel method	$KMnO_4$	500	80–90	Spherical	[110]
21	$CF@CoFe_2O_4@MnO_2$	Sol–gel method and hydrothermal reaction	—	100	750	Fibers shape	[111]
22	$MnCo_2O_4$ nanoparticles	Solvothermal method	—	450	500	Flower-like	[112]
23	Ceria incorporated manganese oxide (NCMO)	Coprecipitationcalcinations and sol–gel methods	—	—	70–90	Spherical	[113]
24	MnO_2	Green synthesis	$KMnO_4$	—	1–60	Spherical	[114]

3.1. Mn^{2+} Ion. Mn^{2+} ion known as manganese ion with a +2 oxidation state indicates the loss of two electrons. Manganese possesses a d^5 electron configuration in its +2 oxidation state that makes it a stable ion and is capable of forming a variety of coordination complexes with ligands. Mn^{2+} is a common oxidation state for manganese and has a d^5 electron configuration in which two of the d electrons occupy the t_{2g} orbitals that possess spherical shape and lower energy, and the other three d electrons occupy the e_g orbitals that own more elongated shape and higher energy. The electronic configuration of Mn^{2+} can be indicated as (Ar) $3d^5$. The coordination number of Mn^{2+} is 6, indicating that it is surrounded by six ligands or atoms in a complex. The most prevalent coordination geometry for Mn^{2+} is octahedral, in which the central Mn^{2+} ion is surrounded by the six ligands at the vertices of an octahedron. The ligands can be either neutral molecules or anions and they interact with the Mn^{2+} ion through coordinate covalent bonds. Ligands are usually water molecules, chloride ions, or other small anions in Mn^{2+} ions.

3.2. Mn^{3+} Ion. Mn^{3+} ion is another oxidation state of manganese with a charge of +3, formed when neutral manganese atoms lose three electrons. The electronic configuration of Mn^{3+} ion is (Ar) $3d^4$ obtained from the neutral state of Mn, (Ar) $3d^5$ $4s^2$ by the loss of three electrons. Mn^{3+} ions are known for their intriguing magnetic properties and are widely utilized in the production of steel. Mn^{3+} ions can be oxidized to a higher oxidation state or reduced to a lower oxidation state by redox reactions. This ionic form exists in minerals or rocks and is also employed as a catalyst for various chemical reactions.

3.3. Mn^{4+} Ions. Mn^{4+} ion possesses an oxidation state of +4 formed when neutral manganese atoms lose four electrons. It follows the electronic configuration of (Ar) $3d^3$ $4s^2$ and expresses good magnetic properties because of the unpaired electrons in 3d orbitals. Generally, Mn^{4+} ion is found in the form of a complex ion in an aqueous solution with the different electronic structure because of its interaction with ligands. In a simple octahedral complex with six ligands, the Mn^{4+} ion would lose all four of its valence electrons from the 3d orbital, leaving only the 4 s electrons with the electronic configuration (Ar) $4s^2$. The electronic structure of Mn^{4+} ions is different in complex ligand environments like tetrahedral or square planar complexes. In some cases, some of the 3d electrons are involved in bonding with the ligands resulting in the partially filled 3d subshell and a modified electronic structure. Thus, the electronic structure of Mn^{4+} ions mainly relies on the particular ligand environment and the nature of the bonding interactions with those ligands. Mn^{4+} ion is found to be highly oxidizing which can accept electrons from other atoms or ions which makes them more suitable in various chemical reactions. Besides, the Mn^{4+} ion is known to be stable under certain conditions and can also be reduced into a lower oxidation state by other species resulting in the formation of other compounds.

The oxidation states of the manganese influence the biocompatibility, imaging, and therapeutic effect by its reactivity, redox properties, and stability [119]. Mn^{2+} ions are considered to be safe than other oxidation states due to their involvement in the enzymatic reactions in the body. The higher oxidation might have increased reactivity which will influence the biocompatibility and also can induce antioxidant behavior [120]. Mn^{2+} ions are good in providing T_1 relaxation enhancement which is favorable for enhancing the signal intensity in MRI. Mn^{3+} is considered to be active in therapeutic effect due to its reactivity in producing reactive oxygen species to scavenge free radicals [121].

4. Medical Applications

Nanoparticles are widely used in different medical applications like drug delivery, imaging, biosensors, MRI, vaccine delivery, antimicrobial applications, wound healing, photothermal therapy, gene therapy, and hyperthermia. In this section, few important medical applications of MnO_x like hyperthermia, MRI, and drug delivery are discussed.

4.1. Hyperthermia. Hyperthermia is an effective therapeutic approach in which the body tissue is exposed to high temperatures ranging from 40 to 45°C for a certain duration. Hyperthermia ruins cancer cells by damaging their protein and DNA leading to cell death. It can enhance the sensitivity of cancer cells to radiation therapy and chemotherapy and provoke the immune system to decimate the cancer cells by the natural defense mechanism. Mn NPs have been explored for their potential in hyperthermia applications, thanks to their unique magnetic and thermal properties. They have the ability to engender heat on exposure to an alternating magnetic field, a property named magnetic hyperthermia. Mn NPs exhibit several advantages over other materials due to their high magnetic moment and biocompatible nature.

Magnetic hyperthermia efficiency is investigated by the specific absorption rate (SAR), which relies on the size, shape, composition, concentration of NPs, and applied magnetic field. A higher SAR value is more favorable as it reduces the dosage and duration of treatment. The necessary therapeutic temperature depends on the size, saturation magnetization (M_s), amplitude, frequency, and time of the applied magnetic field. Generally, ferrites, magnetite, and maghemite are very much employed in hyperthermia studies. Among different ferrites, manganese ferrites are more pertinent for hyperthermia owing to their chemical stability, low inherent toxicity, simple synthesis approach, and exquisite magnetic properties. Besides it is very much suited for MRI and contrast agents. Mn NPs are used as either dopants or combined with other magnetic NPs in hyperthermia studies. Andrade et al. [122] prepared calcium-doped manganese nanoparticles coated with citrate in the range of 10–20 nm by sol–gel approach. It is reported that $Ca_{0.2}Mn_{0.8}Fe_2O_4$ expressed the highest SAR value of 36.3 W/g at low frequency and attained a temperature variation ~7°C in 120 s and corroborated cytocompatibility over 0–250 μg/mL range with good internalization after 24 hr making them more suitable for hyperthermia agent. The magnetic hyperthermia measurements of $MnFe_2O_4$ and $Ca_{0.2}Mn_{0.8}Fe_2O_4$ are shown in Figure 12. Silveira-Alves Jr. et al. [123] reported the preparation of $MnFe_2O_4$, coupled with meso-tetrakis(N-methylpyridinium-4-yl) porphyrin

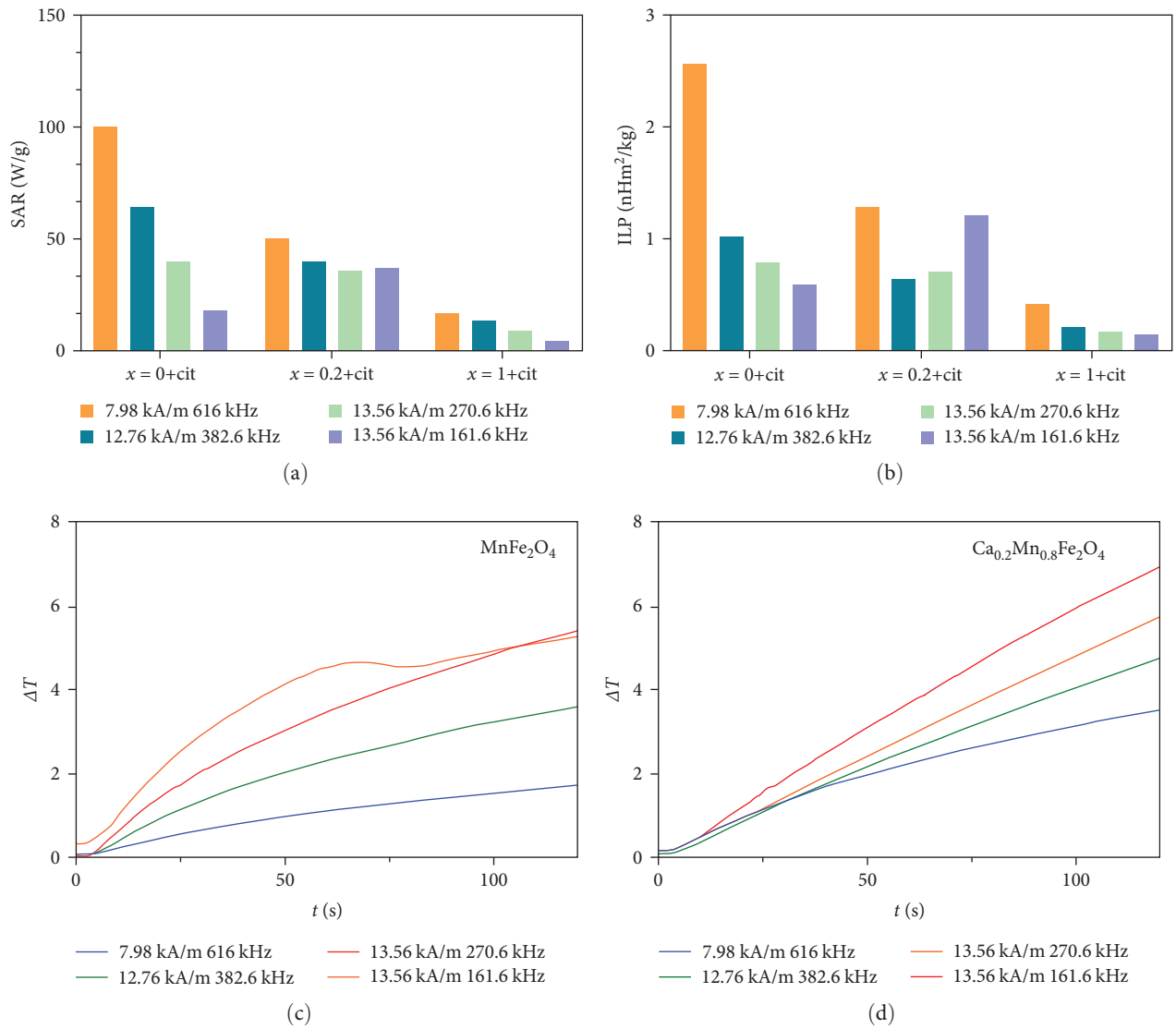

FIGURE 12: (a) Values of SAR, (b) ILP, (c) citrate-functionalized NPs and variation of temperature (ΔT) over time (t) of $MnFe_2O_4$, and (d) $Ca_{0.2}Mn_{0.8}Fe_2O_4$ (reprinted with permission from [122], MDPI, 2022).

(TMPyP) and their zinc complex (ZnTMPyP) and coated with citrate (CA), dimercaptosuccinicnate (DMSA), tripolyphosphate (TPP) anions. The colloidal stability and saturation magnetization of different surfactant-coated $MnFe_2O_4$ NPs are represented in Figure 13. M_s of CA, DMSA, and TPP coated $MnFe_2O_4$ values were found to be 49.6, 45.8, and 43.9 emu/g, respectively. The mild variation in the M_s for different surfactants is because interaction between the capping and the nanoparticles surface alters the spin canting and magnetic order of the nanoparticles. In another work, $MnFe_2O_4$ NPs were modified with polyethylene glycol (PEG) loaded with glucose oxidase and exhibited good magnetic susceptibility with M_s of ~75 emu/g and SAR of 296 W/g [124]. Joshi et al. [125] developed Core@Shell NPs, i.e., γ-Fe_2O_3@Mn_xO_y@SiO_2 by thermolysis of iron and manganese oleate. The hyperthermia studies of the prepared on γ-Fe_2O_3@Mn_xO_y@SiO_2 MCF-7 and A549 cell lines revealed that cell viability is decreased after treating the cells with an AC magnetic field. Gupta and Sharma [126] reported Mn-doped magnetic nanoclusters by hydrothermal synthesis route with SAR value ~600 W/g MNC observed at 250 μg/mL. Phalake et al. [127] stated that $Mn_{0.75}Fe_{0.25}Fe_2O_4$ demonstrated a remarkable SAR value of 153.76 W/g which is due to the substitution of Mn^{2+} in A or B position in the Fe_3O_4 structure. Recently, Shah et al. [128] investigated the lauric acid coated Mn–Zn-based ferrofluid for hyperthermia against HeLa and MG-63. Singh et al. [129] reported that the substitution of Mn^{2+} ions in magnetite distinctly boosted the SAR value (SAR: 510 kW/kg). Hence, the efficiency of manganese-based hyperthermia agents relies on the concentration of Mn^{2+} substitution, site of substitution, particle size, morphology, saturation magnetization, applied magnetic field, frequency, and the dosage of NPs [130]. Some of the manganese-based hyperthermia agents and their SAR values are represented in Table 2.

4.2. Magnetic Resonance Imaging (MRI). MRI is a persuasive noninvasive medical imaging technique in the diagnosis of

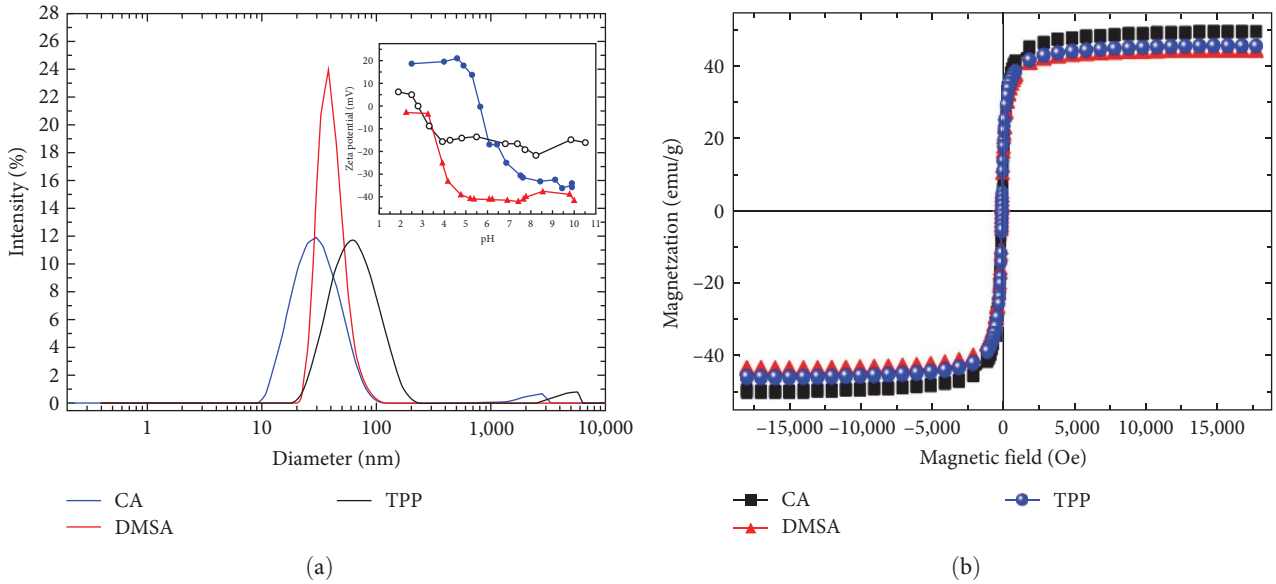

FIGURE 13: (a) Hydrodynamic diameter and ζ potential (inset) of ferrofluids; (b) magnetization curves of $MnFe_2O_4$ (reprinted with permission from [123], Elsevier, 2023).

internal structures of the body. It is exclusively employed in imaging soft tissues like the brain, spinal cord, and muscles to diagnose various medical conditions like cancer, stroke, and neurologic disorders. Nanoparticles like Fe_3O_4 [134–136], Fe_2O_3 [137–139], Fe-based alloy [140], Mn [141–143], and gadolinium-based materials [144–146] are used in MRI as contrast agents. Manganese ions are explored as contrast agents in MRI due to the unpaired electron, making them paramagnetic [147, 148]. This paramagnetic behavior distorts the local magnetic field, inducing a contrast effect in the MRI Image. Furthermore, Mn ions have a prolonged relaxation time than water molecules allowing longer imaging windows, improved signal intensity, and specificity [149, 150]. Mn can impact relaxation times but can act as either a T_1 or T_2 contrast agent, based on its oxidation state and the surrounding environment. This versatility allows manganese to provide contrast in both T_1 and T_2 weighted images, whereas gadolinium-based materials alter the relaxation times by nearby water protons and enhance signal intensity in T_1 weighted images [151, 152]. Besides, Mn^{2+} ions are dominant in the brain cells mitochondria, making them a more suitable candidate for imaging neurodegenerative diseases [153]. Mn can involve in cellullar processes and possess the potential to present insights into functional behavior of tissues and organs, making it favorable for functional MRI (fMRI) applications while Gd-based materials can provide imformation only on structural abnormalites and not the functional aspects of tissues and organs [141, 154]. Mn-based contrast agents are considered to be safe than the other traditional contrast agensts.

Mo et al. [155] reported polydopamine–manganese dioxide MRI-guided photodynamic therapy. As shown in Figure 14, in vitro T_1 weighted imaging studies revealed that the concentration of Mn is in a linear relationship in both acidic and neutral conditions. The brightness of the image was dominant in the acidic state pH = 6.5, then neutral. The T_1 relaxation rate at pH = 6.5 was 4.58 $mm^{-1}\,s^{-1}$, more significant than that in a normal environment. Lopes et al. [156] developed the MnO_2-based hydrogel made of gelatin gum and hyaluronic acid as a contrast agent for MRI. Mn-based MRI techniques are not constrained to diagnosis but could be used as guidance for the therapy. For instance, Hou et al. [157] reported ovalbumin-loaded Mn_3O_4 NPs for dendritic cells-based immunotherapy utilizing the direction of T_1 MRI. The developed system revealed enhanced T_1-MR imaging, ameliorated tumor accumulation, and efficacy in monitoring the real-time treatment procedure. MRI properties and T_1-weighted imaging of ovalbumin-loaded Mn_3O_4 NPs are shown in Figure 15. Mn-based oxides, chelates, and coordination complexes are used as dopants to alter the relaxation times for the improved signal intensity resulting in better image contrast. Cai et al. [158] reported Mn doped silica materials of different dimensions for the MRI visualization. Mn-doped Fe_3O_4 is found to be a strong candidate for resonance imaging techniques; Mn doping decreases the hydrodynamic size and increases the saturation magnetization and magnetic moments resulting in higher r_2 and r_1 due to tenacious spin–spin interactions [159]. PEG-coated Mn-doped Fe_3O_4 NPs possessed hydrophilicity and biocompatibility. It is reported that the prepared ratio of 1 : 20 (Mn : IONP) exhibited harmonious longitudinal and transversal relaxivity of $r_1 = 7.1\,mM^{-1}\,s^{-1}$ and $r_2 = 120.9\,mM^{-1}\,s^{-1}$, respectively, signified that it could be a superior T_1/T_2 dual-contrast MRI [160]. In Mn-doped ZnSe quantum dots on mesoporous silica NPs, improved Mn^{2+} concentration increased T_1 MR contrast resulting in the enriched MRI signal [161]. In some cases, manganese oxide nanoparticles are used as a coating for enhanced MRI. Zhao et al. [162] coated MnO_2 over gold nanorods covered by silica dioxide (SiO_2) and camouflaged myeloid-derived suppressor cells on the surface.

Table 2: Manganese oxides-based hyperthermia agents.

Nanoparticle	Preparation	Size (nm)	Ms (emu/g)	Hc (Oe)	SAR	Applied magnetic field	Cancer	References
Calcium-doped manganese ferrite nanoparticles	Sol–gel method	10–20	—	—	36.3 W/g	7.98 kA/m and 616 kHz	HEK 293T (ATCC CRL-3216)	[122]
$MnFe_2O_4$	Coprecipitation method	37.8	49.6, 45.8, and 43.9	—	—	—	—	[123]
$MnFe_2O_4$	Hydrothermal	21	75	149	296 W/g	150–450 O_e and at a fixed frequency of 316 kHz	HeLa and Saos−2 cancer cell lines	[124]
γ-Fe_2O_3@Mn_xO_y@SiO_2	Thermolysis	25	—	—	—	4 kW	MCF-7, A549	[125]
Mn-doped magnetic clusters	Hydrothermal	34.55 ± 3.41	—	—	~600 W/g MNC (or 2197.80 W/g magnetic content (Fe + Mn))	405 kHz with field amplitude of 168 O_e	—	[126]
$Mn_xFe_{1-x}Fe_2O_4$ ($x = 0-1$)	Chemical coprecipitation	10 ± 0.2– 13 ± 0.2	—	—	153.76 W/g	13.3–26.7 kA/m 277 kHz	—	[127]
$Co_{1-x}Mn_xFe_2O_4$	Coprecipitation	10–50	12.28– 57.4	0.1–6.1	8.9–66.8	30 mT, 342 kHz	—	[131]
Caffeine-based N-heterocyclic carbene silver complex magnetic nanoparticles	—	—	75	—	180.97	335.2 O_e	—	[132]
PEG-$CoFe_2O_4$	Combustion method	25 and 28	82.87	1,229	—	—	—	[133]

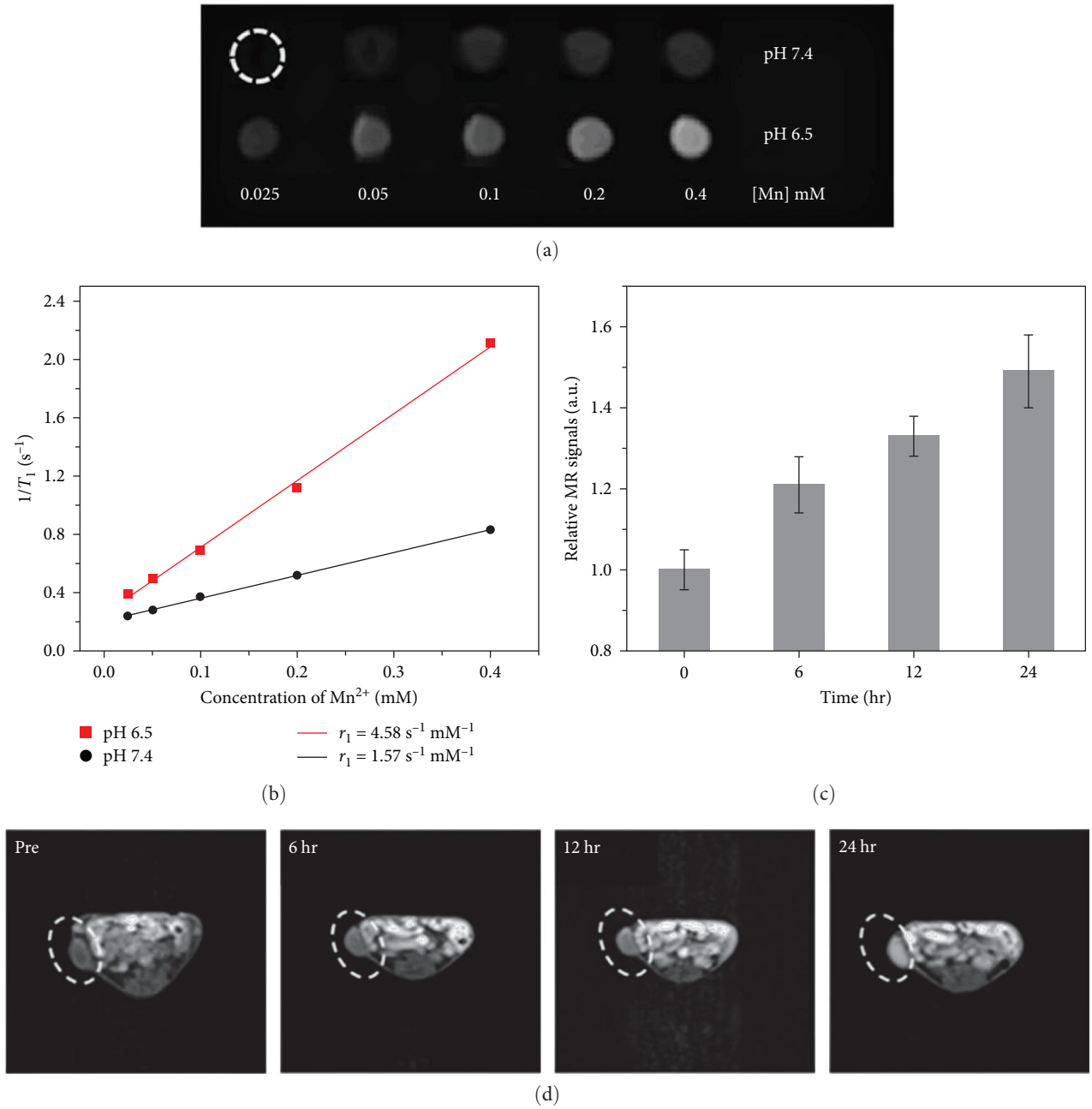

FIGURE 14: (a) In vitro $T1$-MR imaging of PMIDA NPs with different concentrations of Mn^{2+} (0.025, 0.05, 0.1, 0.2, and 0.4 mM) was performed; (b) linear fitting of Mn^{2+} concentration and $1/T_1$ of PMIDA NPs; (c) corresponding normalized signal intensity enhancement of the $T1$-weighted MR signals in the $4T_1$ tumor section; and (d) in vivo MR images of $4T_1$ tumor-bearing mice pre- and post-intravenous injection of PMIDA NPs dispersions (reprinted with permission from [155], Elsevier).

It is reported that the release of Mn^{2+} in an acidic tumor microenvironment makes it favorable for the MRI. Shi et al. [163] coated MnO_2 and AuNP on mesoporous Prussian blue for MRI and antitumor therapy, and the release of Mn^{2+} ions from the degradation of MnO_2 upgraded MR relaxation. Recently, nanodiamonds doped with Mn were reported by Kunuku et al. [164]. The doping of Mn on nanodiamonds improved the relaxivity, i.e., longitudinal and transversal relaxivity was 5 and 17 times higher than the pure nanodiamond. Thus, manganese can be used as a dopant, coating for enhanced resonance imaging. It can be combined with other magnetic materials for better T_1/T_2 contrast images. Drug loading and surface modification of manganese oxides make them more suitable for live diagnosing guidance for the treatment. The stability and the dosage of the Mn-based material are required to explore more Mn-based materials for MRI.

4.3. Drug Delivery. Manganese oxides are extensively used for drug delivery applications due to their exclusive properties like

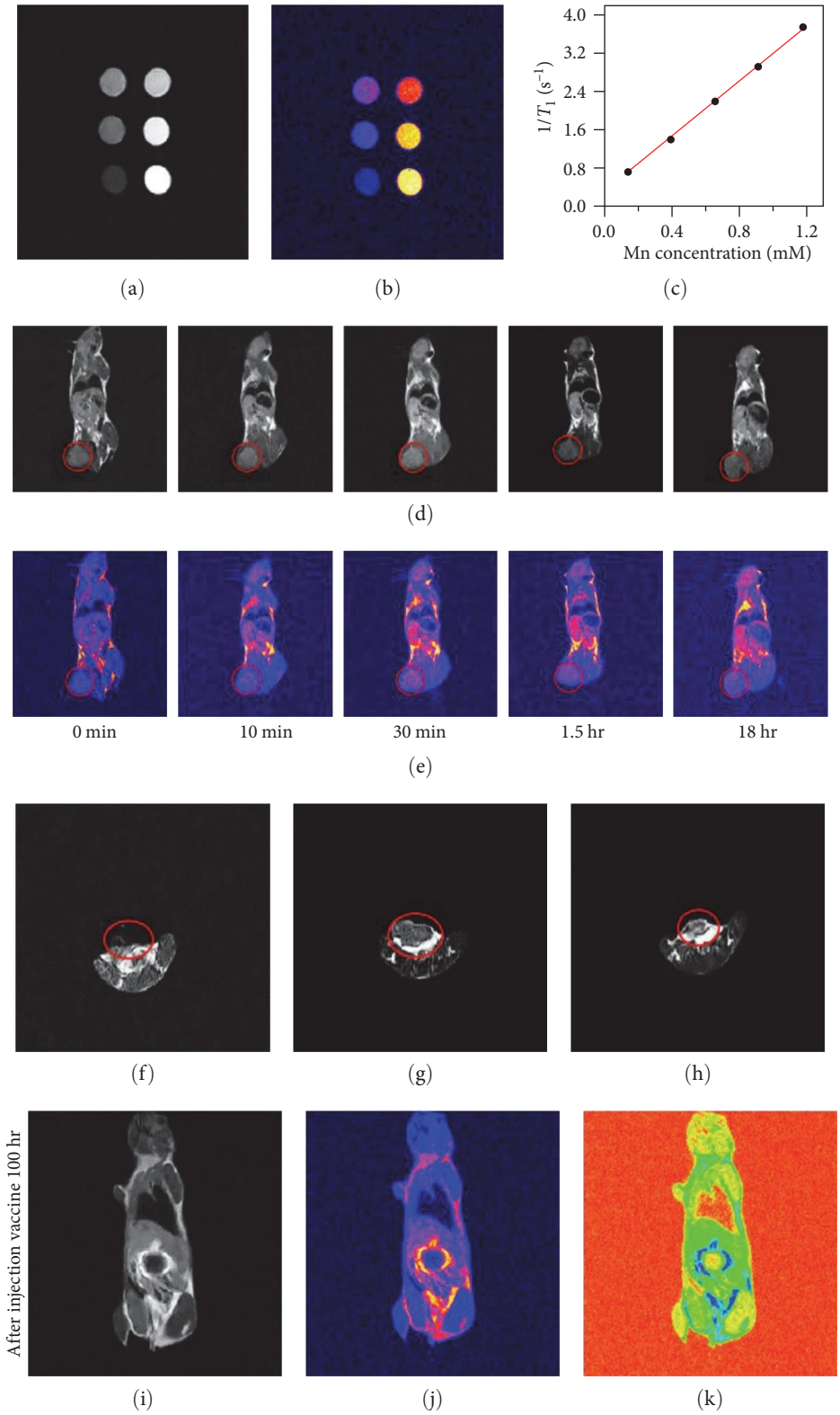

Figure 15: MRI properties of ovalbumin loaded Mn_3O_4 NPs: (a, b) $T1$-weighted MR imaging in comparison to water, (c) a plot of the longitudinal ($T1$) relaxation rates of the prepared Mn_3O_4@PF68-OVA NV nanoprobes against different Mn concentrations, (d) $T1$-weighted MR images of a mouse before injection and 10, 30, 60 min, 1.5, and 18 hr postinjection, (e) the pseudo color images corresponding to (d, f) cross-section $T1$-weighted MR images in the control group and (g, h) $T1$-weighted MR images of a mouse before and 24, 48 hr of postsubcutaneous injection, and (i) in vivo MR imaging with (j, k) the pseudo-color images corresponding to (d) after 100 hr of vaccination (reprinted with permission from [157], Elsevier, 2023).

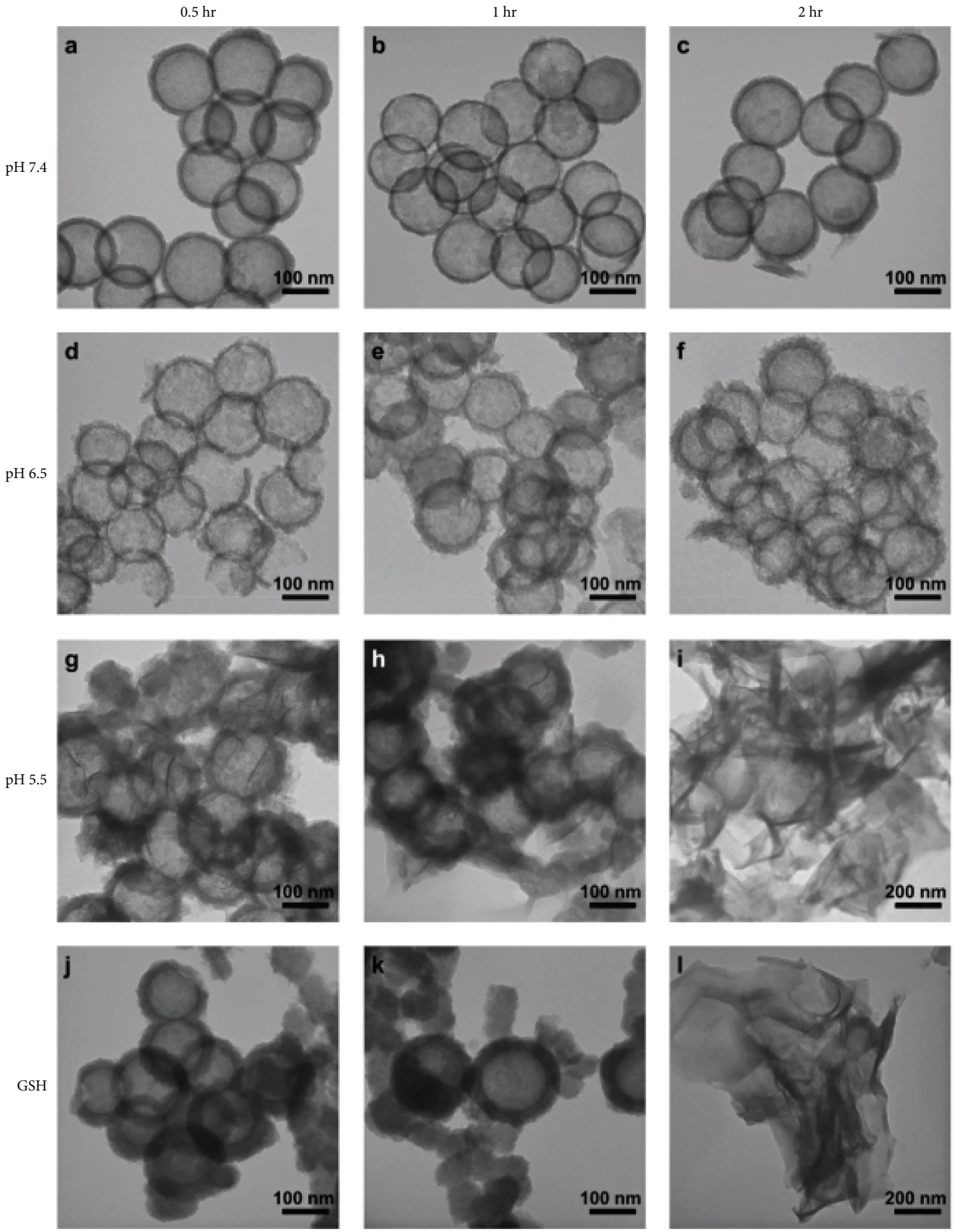

Figure 16: (a–l) TEM image of DOX loaded HMDN functionalized with PEI and PLL at different pH and GSH concentration (reproduced with permission from [178], Elsevier).

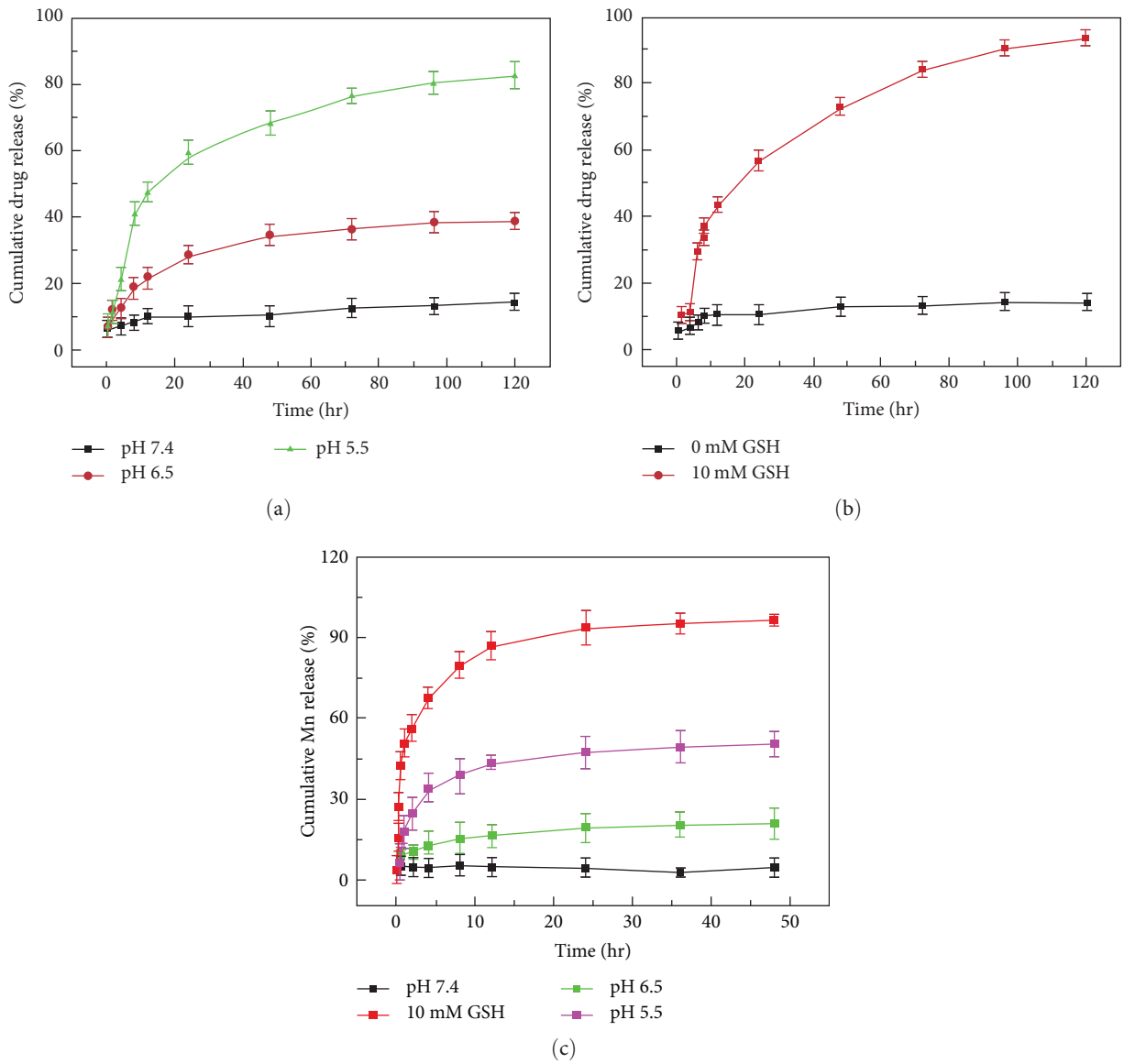

Figure 17: Cumulative release of DOX from DOX@HMDN-PEI-PLL(cit) at different pH values (5.5, 6.5, and 7.4) (a) and different GSH concentrations (0 and 10 mM) (b) and cumulative release of Mn from DOX@HMDN-PEI-PLL(cit) at different pH values (5.5, 6.5, and 7.4) and different GSH concentrations (0 and 10 mM) (c) at 37°C (reprinted with permission from [178], Elsevier).

biocompatibility, high surface area, redox activity, stimuli–responsive, and tunable surface [121, 165, 166]. The Mn oxides are used in drug delivery in different forms like MnO_2 [167], MnO [168], Mn_2O_3 [169], Mn_3O_4 [34], and Mn-based composites [170, 170]. Mn NP is used in different structures like rods [171], spheres [166], wires [172], sheets [173], platelets [174], mesoporous [166], hollow [175], etc. The redox ability of MnO_2 makes it more favorable for the triggered drug release by the reversible redox reaction [176]. Mn-based NPs are capable of undergoing a Fenton reaction, where Mn ions initiate the decomposition of H_2O_2 present in the tumor environment and generate oxygen and increase the reactive oxygen species in cancer cells resulting in the activation of oxidative stress which ruins cancer cells [177]. Xu et al. [178] reported the doxorubicin (DOX) loaded hollow MnO_2 NPs (HMDN) functionalized with polyethyleneimine (PEI) and polylysine (PLL) (DOX@HMDN-PEI-PLL(cit)) for chemo-hemodynamic cancer therapy. It is reported that the decomposition of hollow manganese oxide nanoparticles into Mn^{2+} ion under acidic conditions and high glutathione (GSH) concentration provoked the release of DOX and Fenton like reaction for the augmented therapeutic effect. The TEM image and drug release behavior of DOX@HMDN-PEI-PLL at different pH and GSH is represented in Figures16 and 17. C6 cell membrane coated DOX conjugated MnO_2 system is used for the treatment of glioma by inducing oxidative stress for the destruction of cancer cells via the Fenton reaction [179]. He et al. [180] prepared the honeycomb-structured hollow MnO_2 carrier of ~93 nm using template-assisted synthesis approach for the delivery of DOX. The hollow MnO_2 carrier comprised some MnO_2 platelets which facilitates the adsorption of DOX by the van der Waals interaction between drug

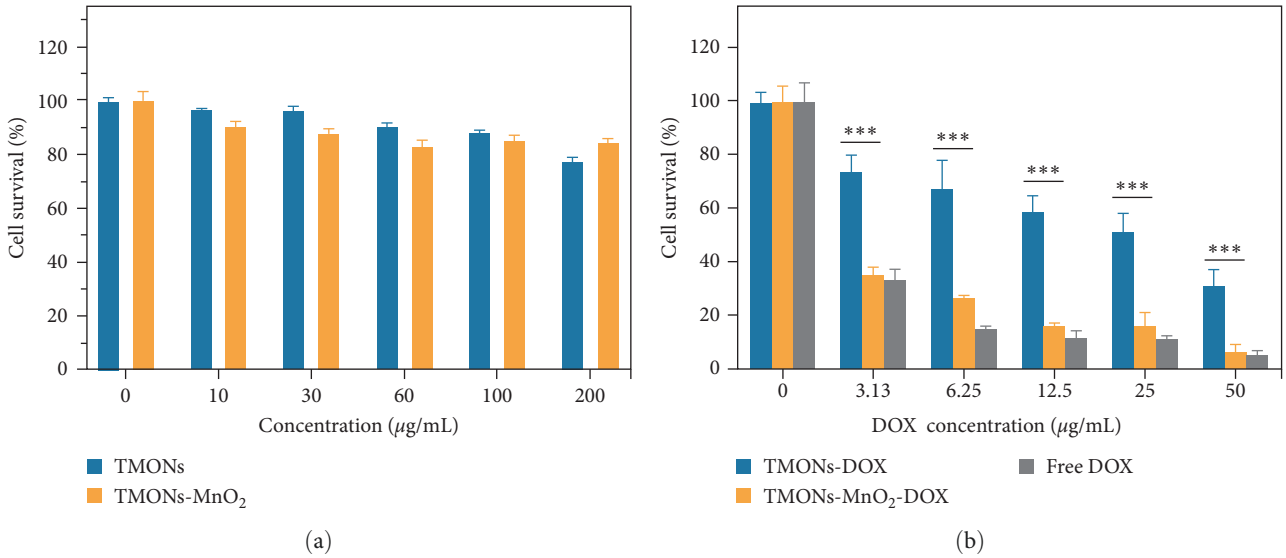

FIGURE 18: (a) Cell survival rate of TMONs and TMONs-MnO_2 coincubated with 4*T*1 breast cancer cells for 24 hr; (b) the cell survival rate of free DOX, TMONs@DOX, and TMONs-MnO_2@DOX after coincubation with 4*T*1 breast cancer cells for 24 hr $^{***}P<0.001$ (reproduced with permission from [187], Elsevier).

molecules and MnO_2. It is reported that the MnO_2 carrier was withered to Mn^{2+} in the GSH environment for the release of DOX via thiol-mediated reduction. Drug release studies revealed that around 100% of DOX released in 15 min in GSH. Tan et al. [181] reported DOX-loaded MnO_2 zeolitic imidazolate framework-8 for the treatment of lung cancer. The amount of drug released was varied with pH, i.e., total amount of drug released at different pH 7.4, 6.0, and 5.0 is 15%, 53%, and 82%, respectively. MnO NPs are utilized in drug delivery due to their dexterity toward surface modification for the targeted delivery. Mesoporous structures are more welcomed in the drug delivery due to their drug-loading capacity and surface functionalization ability. Zhang et al. [182] used mesoporous MnO_2 as a carrier to load the histone deacetylase inhibitor and covered with polydopamine, functionalized with ruthenium nitrosyl donor (Ru-NO) and a folic acid (FA) for the enhanced site-specific delivery and improved therapeutic effect. Zheng et al. [183] developed the PEG functionalized MnO NPs conjugated Cy 5.5 as an MRI guided drug delivery system for myocardial infarction. Mn_3O_4 NPs have been explored for controlled drug release studies as they can undergo redox reactions exclusively the interconversion between Mn(II) and Mn(III) oxidation states. The redox activity facilitates the drug release in response to stimuli like pH and reducing agents. Besides Mn_3O_4, NPs are functionalized with ligands and targeting moieties for the enhanced recognition of target cells and site-specific delivery of drugs. Jain et al. [184] reported the biotin functionalized PEG modified Mn_3O_4 nanocuboids for the delivery of gemcitabine to target breast cancer cells. Serotonin-stearic acid bioconjugated Mn_3O_4 nanocuboids for the delivery of doxorubicin to liver cancer cells. The formulation exhibited 98.3% drug encapsulation with 22.9% loading efficiency and showed higher drug release in acidic media signifying a good therapeutic system [109]. Zhou et al. [185] developed DOX-loaded Mn_3O_4@Au conjugated with double stranded DNA to activate the stimulator of interferon genes (STING) which synergistic antitumor activity by the combination of phagocytosis due to STING and chemotherapy due to DOX. Arjama et al. [186] reported that Mn_2O_3 nanoparticles are used as templates to prepare the dopamine loaded hyaluronic acid and chitosan hydrogels. Mn-based composites and hybrid nanoparticles gained much attention to extend the drug-loading ability, the optimized drug release, site-specific delivery to enhance biocompatibility. Manganese oxides are combined with mesoporous organosilica (TMON) for the delivery of DOX and to improve the biodegradability and biocompatibility. It is reported that the Mn-based hybrid with silica particles facilitates the cell membrane crossing and delivers the drug resulting in improved cancer cell death [187]. The cytotoxic activity of TMON-MnO_2 and TMON-MnO_2-DOX are shown in Figure 18. Mn is combined with upconversion nanoparticles and metal–organic framework for the delivery of 3-F-10-OH-evodiamine (FOE), an antitumor agent [188]. Recently, Sabaghi et al. [189] prepared chitosan crosslinked tripolyphosphate-coated MnO_2 rod to achieve the biocompatibility and labeled with fluorescein isothiocyanate for the targeted delivery of doxorubicin to the tumor microenvironment. Mn-based materials are high potential in delivering drugs to the targeted site and are capable of enhancing the therapeutic effect by combined therapy and MRI-guided therapy. The improved therapeutic effect of Mn-based drug delivery depends on the size and morphology of the carrier, drug-loading capacity, redox reaction, Fenton reaction, stimuli–responsive behavior, and biocompatibility, etc. More attention has to be given to controlling the dosage level, surface functionalization, and controlled drug release behavior. Some of the recently prepared Mn-based oxides as a drug delivery carriers are presented in Table 3 [109, 155, 178, 179, 181, 184, 187, 188, 190–197].

(1) Other Applications. Mn-based materials are also harnessed for other medical applications like wound healing, antioxidant agents, antimicrobial agents, and biosensing applications. Mn-based nanomaterials are known for their

Table 3: Manganese oxides-based drug delivery carrier.

S. no.	Nanoformulation	Preparation method	Size (nm)	PDI (mV)	Zeta potential (mV)	Drug	Drug-loading efficiency (%)	Drug encapsulation efficiency (%)	Drug release (%)	Disease	References
1	Polydopamine–manganese dioxide-IR780 iodide	Self-polymerization	244.6	0.172	−19.5 ± 1	Polydopamine	97.5	9.18	—	—	[155]
2	Hollow MnO_2	Reduction	—	—	—	Doxorubicin	20.0	50.2	38.7	HeLa, MCF-7	[178]
3	MnO_2-DOX-C_6	Reduction	55.34 ± 2.93	0.212	27.30 ± 2.11	Doxorubicin	—	—	66.84 ± 3.8	—	[179]
4	DOX/MnO_2@ZIF-8[c]	—	206.22 ± 21.00 nm	—	—	Doxorubicin	12	—	82	Lung cancer	[181]
5	Biotin–PEG Mn_3O_4 nanocuboids	—	—	—	—	Gemcitabine	—	—	—	Breast cancer	[184]
6	Mno_2 dopped triple hybrid mesoporous organosilica nanoparticles	Sol–gel method	271	—	−6.98	Doxorubicin	—	13.5	—	Breast cancer	[187]
7	DUCNP@Mn−MOF/FOE	—	—	—	—	3-F-10-OH-Evodiamine	83	—	—	—	[188]
8	ST-SA@MNCs[b]	Chemical precipitation	21 nm	—	−15	Doxorubicin hydrochloride	—	—	81.4 ± 1.6	HePG2	[109]
9	DOX@(hPDA/MnO_2)-PEG	—	23.6	—	−22.6	Doxorubicin	—	—	43	—	[190]
10	Hollow MnO_2	—	100	—	−22	Doxorubicin	94.67	—	—	—	[191]
11	tLyP-1-CD-DOPA-MnO_2@PTX[a]	137.0 ± 1.9	—	16.0 ± 1.3	—	Paclitaxel	—	—	—	Orthotopic glioma	[192]
12	Aptamer mediated hollow MnO_2	100 ± 10	—	33.84–36.06	—	Sorafenib	22	88	18	Liver cancer	[193]
13	Mn_3O_4@PAA@ZIF-8/MTX	Hydrothermal	—	—	—	Methotrexate	80	—	53	BT-474 and MCF-7	[194]
14	AuNPs@$MnCO_3$/Mn_3O_4	—	—	—	—	Doxorubicin and propium iodide	—	—	—	Breast cancer	[195]
15	Hollow MnO_2	—	129 nm	—	−27	Bufalin	28.6 ± 3.5	80.0 ± 4.3	81 ± 2	H22	[196]
16	Au/MnO_2	—	146 nm	—	+13.6	Doxorubicin	99.1	—	25	—	[197]

[a]tLyP-1-CD-DOPA-MnO_2@PTX, tLyP-1-modified dopamine (DOPA), β-cyclodextrin (CD)-coated paclitaxel (PTX), and manganese dioxide (MnO_2)-loaded nanoparticles. [b]ST-SA@MNCs—serotonin–stearic acid-based bioconjugate modified manganese oxide-based nanocuboids. [c]DOX/MnO_2@ZIF-8—doxorubicin-loaded MnO_2@Zeolitic Imidazolate Framework-8.

favorable antimicrobial effects encompassing antibacterial and antifungal prompting widespread research attention. For instance, Lu et al. [86] reported that MnO_2 nanoparticles synthesized using the extract of *V. betonicifolia* showed better antibacterial, antifungal, and antioxidant activity. The antibacterial activity of MnO_2 is due to the production of reactive oxygen species which induces oxidative stress in the bacterial cell and the interaction of the nanoparticles to the surface of the bacterial cells. Farhan and Mohammed [198] evaluated the efficacy of MnO_2 NPs for antioxidant and antidiabetic agents due to the production of reactive oxygen species, high surface area to volume ratio, and catalytic activity. Pardhiya et al. [199] investigated the bovine serum albumin conjugated MnO_2 nanoparticles as antioxidant nanozymes and the efficiency increased with nanoparticle concentration. Recently, Zhang et al. [200] investigated that the BSA-coated MnO_2 nanoparticles demonstrated catalase (CAT), superoxide dismutase (SOD), and glutathione peroxidase mimicking activities. The antimicrobial and antioxidant properties of Mn-based materials are improved by doping with nanoparticles like silver [201], gold [202], and functionalization with polymers [203], ligands [204], and antibodies [205]. Liu et al. [206] reported that the oleic acid-coated MnO_2 eradicated biofilm formation of staphylococcus aureus and demonstrated supreme antibacterial performance compared to vancomycin and the reactive oxygen therapy of OA-MnO_2 promoted wound healing in mice. Mn-based nanomaterials are used in photodynamic therapy due to their oxidation properties which assist in mitigating the hypoxic condition of the tumor microenvironment by interacting with the H_2O_2 found in tumors [207]. Deng et al. [197] fabricated photosensitizer functionalized Mn@Co magnetic nanoparticles for photothermal therapy of gastric cancer. Ijaz Dar et al. [208] reported that the Au@Mn_3O_4 magnetoplasmonic nanoflowers exhibited noticeable photothermal heating effect with 38% of thermal transduction efficiency than Au nanorods and nanoparticles. Moreover, Mn-based nanostructures are explored as biosensors and fluorescent quenchers. Especially 2d manganese nanostructures are good in light harvesting and conducting electrons making them more favorable for sensing in both biological and chemical applications [209]. Chauhan et al. [210] reported Au coated 2d material wrapped MnO_2 nanocomposite for the sensing of neurotransmitter acetylcholine. Recently, Gao et al. [211] investigated MnO_2 nanosheets-based sensor for the determination of staphylococcus aureus which causes food-borne diseases. Therefore, all these examples signify that manganese-based materials could hold significant promise in medicinal applications.

5. Issues and Challenges

Though manganese oxides are blooming in medical applications, it is challenging to ascertain the degree of toxicity associated with the various oxide phases. The biocompatibility of Mn-based material varies with the oxidation states. The accumulation and neurotoxicity of manganese are a major threat to be used in biological systems. More studies like in vivo experiments are recommended in determining the dosage of the nanoparticles to avoid toxicity and neurotoxicity. The transformation of manganese-based materials from laboratory to clinical market requires a systematic methodology for determining the correlation between the formulations of Mn-based materials and the in vivo pharmacokinetics and long-term toxicity assessment of NPs. Though the multioxidation states of the Mn-based nanoparticles are highly reactive in scavenging free radicals, stability is the major challenge. More research has to be conducted on the optimization of surface stability by surface functionalization. Economic viability and reproducibility are the other challenges to initiating the commercialization and the utilization in the clinical market.

6. Conclusion

Mn-based magnetic materials hold a huge place in medicinal applications due to the biocompatibility, biological activity, magnetic nature, redox behavior, and availability. Several studies showed that they are toxic to the central nervous system. The enhancement of biocompatibility of Mn-based magnetic particles is of great concern to extend the usage widely in medical applications. The biocompatibility of the Mn-based material can be enhanced by surface functionalization or incorporating other compatible materials, reducing the dosage and optimizing the size and shape. More attention has to be given to conducting the in vivo studies of Mn-based materials in all the applications like MRI, hyperthermia, and drug delivery to optimize the dosage and concentration and analyze the suitable morphology. The development of simple approaches for the preparation of Mn NPs and Mn-based composites on a large scale has to be considered for the production of stable NPs with optimized size and structure. In conclusion, Mn-based magnetic materials are the most promising material in medicinal applications exclusively MRI and drug delivery and more studies have to be conducted for hyperthermia. We believe that this review will serve the researchers to explore the unexplored sides of Mn-based magnetic materials for medicinal applications as they hold a preeminent place in biomedical applications.

Conflicts of Interest

The authors declare that they have no conflicts of interest.

Acknowledgments

Rajesh Kumar Manavalan thanks the contract no. 40/is2. Rajesh Kumar Manavalan and Alexey Sergeevich Volegov gratefully acknowledge research funding from the Ministry of Science and Higher Education of the Russian Federation (Ural Federal University project within the Priority 2030 Program).

References

[1] S. K. Murthy, "Nanoparticles in modern medicine: state of the art and future challenges," *International Journal of Nanomedicine*, vol. 2, no. 2, pp. 129–141, 2007.

[2] K. Cho, X. Wang, S. Nie, Z. Chen, and D. M. Shin, "Therapeutic nanoparticles for drug delivery in cancer," *Clinical Cancer Research*, vol. 14, no. 5, pp. 1310–1316, 2008.

[3] P. Sharma, S. Brown, G. Walter, S. Santra, and B. Moudgil, "Nanoparticles for bioimaging," *Advances in Colloid and Interface Science*, vol. 123-126, pp. 471–485, 2006.

[4] K. Arvinder, K. Deepali, B. Singh, and A. Saroj, "Seclusion of vasicine-an quinazoline alkaloid from bioactive fraction of *Justicia adhatoda* and its antioxidant, antimutagenic and anticancerous activities," *Journal of Global Biosciences*, vol. 5, no. 4, pp. 3836–3850, 2016.

[5] J.-L. Bridot, D. Stanicki, S. Laurent et al., "New carboxysilane-coated iron oxide nanoparticles for nonspecific cell labelling," *Contrast Media & Molecular Imaging*, vol. 8, no. 6, pp. 466–474, 2013.

[6] H. Tian, J. Chen, and X. Chen, "Nanoparticles for gene delivery," *Small*, vol. 9, no. 12, pp. 2034–2044, 2013.

[7] R. Eivazzadeh-Keihan, E. Bahojb Noruzi, K. Khanmohammadi Chenab et al., "Metal-based nanoparticles for bone tissue engineering," *Journal of Tissue Engineering and Regenerative Medicine*, vol. 14, no. 12, pp. 1687–1714, 2020.

[8] Y. Song, X. Huang, Z. Gao, X. Li, and Y. Ma, "Nanoindentation creep behavior of RPV's weld joint at room temperature," *Mechanics of Time-Dependent Materials*, vol. 24, no. 3, pp. 253–263, 2020.

[9] A. I. Ribeiro, A. M. Dias, and A. Zille, "Synergistic effects between metal nanoparticles and commercial antimicrobial agents: a review," *ACS Applied Nano Materials*, vol. 5, no. 3, pp. 3030–3064, 2022.

[10] X. Jiang, A. V. Kuklin, A. Baev et al., "Two-dimensional MXenes: from morphological to optical, electric, and magnetic properties and applications," *Physics Reports*, vol. 848, pp. 1–58, 2020.

[11] M. Kang, J. Hong, M. Jung et al., "T-cell-mimicking nanoparticles for cancer immunotherapy," *Advanced Materials*, vol. 32, no. 39, 2, 2020.

[12] J. Boken, S. K. Soni, and D. Kumar, "Microfluidic synthesis of nanoparticles and their biosensing applications," *Critical Reviews in Analytical Chemistry*, vol. 46, no. 6, pp. 538–561, 2016.

[13] Y. Wei, L. Quan, C. Zhou, and Q. Zhan, "Factors relating to the biodistribution & clearance of nanoparticles & their effects on *in vivo* application," *Nanomedicine*, vol. 13, no. 12, pp. 1495–1512, 2018.

[14] N. Pradhan, S. Das Adhikari, A. Nag, and D. D. Sarma, "Luminescence, plasmonic, and magnetic properties of doped semiconductor nanocrystals, angew," *Angewandte Chemie International Edition*, vol. 56, no. 25, pp. 7038–7054, 2017.

[15] M. Nikzamir, A. Akbarzadeh, and Y. Panahi, "An overview on nanoparticles used in biomedicine and their cytotoxicity," *Journal of Drug Delivery Science and Technology*, vol. 61, Article ID 102316, 2021.

[16] A. F. Burlec, A. Corciova, M. Boev et al., "Current overview of metal nanoparticles' synthesis, characterization, and biomedical applications, with a focus on silver and gold nanoparticles," *Pharmaceuticals*, vol. 16, no. 10, Article ID 1410, 2023.

[17] J. Liu, C. Chen, and Y. Zhao, "Progress and prospects of graphdiyne-based materials in biomedical applications," *Advanced Materials*, vol. 31, no. 42, Article ID 1804386, 2019.

[18] G. G. Flores-Rojas, F. López-Saucedo, R. Vera-Graziano, E. Mendizabal, and E. Bucio, "Magnetic nanoparticles for medical applications: updated review," *Macromol*, vol. 2, no. 3, pp. 374–390, 2022.

[19] D. Yoo, J.-H. Lee, T.-H. Shin, and J. Cheon, "Theranostic magnetic nanoparticles," *Accounts of Chemical Research*, vol. 44, no. 10, pp. 863–874, 2011.

[20] L. S. Arias, J. Pessan, A. Vieira, T. Lima, A. Delbem, and D. Monteiro, "Iron oxide nanoparticles for biomedical applications: a perspective on synthesis, drugs, antimicrobial activity, and toxicity," *Antibiotics*, vol. 7, no. 2, Article ID 46, 2018.

[21] H. Kahil, A. Faramawy, H. El-Sayed, and A. Abdel-Sattar, "Magnetic properties and SAR for gadolinium-doped iron oxide nanoparticles prepared by hydrothermal method," *Crystals*, vol. 11, no. 10, Article ID 1153, 2021.

[22] R. B. Dhanakotti, V. Kaliyamoorthy, K. B. Mane Prabhu et al., "Structural and magnetic properties of cobalt-doped iron oxide nanoparticles prepared by solution combustion method for biomedical applications," *International Journal of Nanomedicine*, vol. 10, pp. 189–198, 2015.

[23] J. A. Joseph, S. B. Nair, S. S. John, S. K. Remillard, S. Shaji, and R. R. Philip, "Zinc-doped iron oxide nanostructures for enhanced photocatalytic and antimicrobial applications," *Journal of Applied Electrochemistry*, vol. 51, no. 3, pp. 521–538, 2021.

[24] M. Zhang, Y. Cao, L. Wang, Y. Ma, X. Tu, and Z. Zhang, "Manganese doped iron oxide theranostic nanoparticles for combined T_1 magnetic resonance imaging and photothermal therapy," *ACS Applied Materials & Interfaces*, vol. 7, no. 8, pp. 4650–4658, 2015.

[25] S. Pal Singh, A. Kumari Singh, and J. Gupta, "Synthesis of nickel-doped iron oxide nanoparticles by co-precipitation method and investigation of its structural and opto-electronic properties," *Materials Today: Proceedings*, vol. 66, pp. 1890–1896, 2022.

[26] S. K. Ghosh, "Diversity in the family of manganese oxides at the nanoscale: from fundamentals to applications," *ACS Omega*, vol. 5, no. 40, pp. 25493–25504, 2020.

[27] Y. Chen, H. Cong, Y. Shen, and B. Yu, "Biomedical application of manganese dioxide nanomaterials," *Nanotechnology*, vol. 31, no. 20, Article ID 202001, 2020.

[28] C. Ling and R. Zhang, "Manganese dioxide as rechargeable magnesium battery cathode," *Frontiers in Energy Research*, vol. 5, Article ID 30, 2017.

[29] H. Hassan, M. W. Iqbal, A. M. Afzal, S. M. Wabaidur, A. M. Tawfeek, and M. Z. Ansari, "AgCo-MOF/MnS deposited on carbonized wood substrate: pioneering the future of supercapacitors and oxygen evolution reactions," *Energy & Fuels*, vol. 37, no. 20, pp. 16072–16086, 2023.

[30] H. Rafique, M. W. Iqbal, H. Hassan et al., "Green synthesis and performance evaluation of MnCuS-GQDs for energy storage systems: a comparative study," *Diamond and Related Materials*, vol. 139, Article ID 110297, 2023.

[31] J. De Rudder, T. Van De Wiele, W. Dhooge, F. Comhaire, and W. Verstraete, "Advanced water treatment with manganese oxide for the removal of 17α-ethynylestradiol (EE2)," *Water Research*, vol. 38, no. 1, pp. 184–192, 2004.

[32] B. Ammundsen, D. J. Jones, J. Rozière, H. Berg, R. Tellgren, and J. O. Thomas, "Ion exchange in manganese dioxide spinel: proton, deuteron, and lithium sites determined from neutron powder diffraction data," *Chemistry of Materials*, vol. 10, no. 6, pp. 1680–1687, 1998.

[33] F. Pei, X. Cao, Y. Sun, J. Kang, Y. X. Ren, and J. Ge, "Manganese dioxide eliminates the phytotoxicity of aerobic compost products and converts them into a plant friendly organic fertilizer," *Bioresource Technology*, vol. 373, Article ID 128708, 2023.

[34] X. Cai, Q. Zhu, Y. Zeng, Q. Zeng, X. Chen, and Y. Zhan, "Manganese oxide nanoparticles as MRI contrast agents in tumor multimodal imaging and therapy," *International Journal of Nanomedicine*, vol. 14, pp. 8321–8344, 2019.

[35] J. Li, C. Wu, P. Hou, M. Zhang, and K. Xu, "One-pot preparation of hydrophilic manganese oxide nanoparticles as T1 nano-contrast agent for molecular magnetic resonance imaging of renal carcinoma in vitro and in vivo," *Biosensors and Bioelectronics*, vol. 102, pp. 1–8, 2018.

[36] J. E. Post, "Manganese oxide minerals: crystal structures and economic and environmental significance," *Proceedings of the National Academy of Sciences*, vol. 96, no. 7, pp. 3447–3454, 1999.

[37] A. Byström and A. M. Byström, "The crystal structure of hollandite, the related manganese oxide minerals, and α-MnO_2," *Acta Crystallographica*, vol. 3, no. 2, pp. 146–154, 1950.

[38] D. A. Kitchaev, S. T. Dacek, W. Sun, and G. Ceder, "Thermodynamics of phase selection in MnO_2 framework structures through alkali intercalation and hydration," *Journal of the American Chemical Society*, vol. 139, no. 7, pp. 2672–2681, 2017.

[39] J. E. Post, D. A. McKeown, and P. J. Heaney, "Raman spectroscopy study of manganese oxides: tunnel structures," *American Mineralogist*, vol. 105, no. 8, pp. 1175–1190, 2020.

[40] S. Turner and P. R. Buseck, "Manganese oxide tunnel structures and their intergrowths," *Science*, vol. 203, no. 4379, pp. 456–458, 1979.

[41] Q. Feng, K. Yanagisawa, and N. Yamasaki, "Hydrothermal soft chemical process for synthesis of manganese oxides with tunnel structures," *Journal of Porous Materials*, vol. 5, no. 2, pp. 153–162, 1998.

[42] L. Kang, M. Zhang, Z.-H. Liu, and K. Ooi, "IR spectra of manganese oxides with either layered or tunnel structures," *Spectrochimica Acta Part A: Molecular and Biomolecular Spectroscopy*, vol. 67, no. 3-4, pp. 864–869, 2007.

[43] R. N. De Guzman, A. Awaluddin, Y.-F. Shen et al., "Electrical resistivity measurements on manganese oxides with layer and tunnel structures: birnessites, todorokites, and cryptomelanes," *Chemistry of Materials*, vol. 7, no. 7, pp. 1286–1292, 1995.

[44] A. G. Newton and K. D. Kwon, "Classical mechanical simulations of layer-and tunnel-structured manganese oxide minerals," *Geochimica et Cosmochimica Acta*, vol. 291, pp. 92–109, 2020.

[45] J. E. Post, D. A. McKeown, and P. J. Heaney, "Raman spectroscopy study of manganese oxides: layer structures," *American Mineralogist*, vol. 106, no. 3, pp. 351–366, 2021.

[46] Q. Feng, K. Yanagisawa, and N. Yamasaki, "Transformation of manganese oxides from layered structures to tunnel structures," *Chemical Communications*, no. 14, pp. 1607-1608, 1996.

[47] F. V. Chukhrov, V. A. Drits, A. I. Gorshkov, B. A. Sakharov, and Y. P. Dikov, "Structural models of vernadite," *International Geology Review*, vol. 29, no. 11, pp. 1337–1347, 1987.

[48] M. O'keeffe, "Cation valencies and distributions in spinel structures containing manganese," *Journal of Physics and Chemistry of Solids*, vol. 21, no. 3-4, pp. 172–178, 1961.

[49] S. Dey and V. V. Praveen Kumar, "The performance of highly active manganese oxide catalysts for ambient conditions carbon monoxide oxidation," *Current Research in Green and Sustainable Chemistry*, vol. 3, Article ID 100012, 2020.

[50] H. Wang, J. Deng, Y. Chen, F. Xu, Z. Wei, and Y. Wang, "Hydrothermal synthesis of manganese oxide encapsulated multiporous carbon nanofibers for supercapacitors," *Nano Research*, vol. 9, no. 9, pp. 2672–2680, 2016.

[51] G. Qiu, H. Huang, S. Dharmarathna, E. Benbow, L. Stafford, and S. L. Suib, "Hydrothermal synthesis of manganese oxide nanomaterials and their catalytic and electrochemical properties," *Chemistry of Materials*, vol. 23, no. 17, pp. 3892–3901, 2011.

[52] X. Wang and Y. Li, "Synthesis and formation mechanism of manganese dioxide nanowires/nanorods," *Chemistry—A European Journal*, vol. 9, no. 1, pp. 300–306, 2003.

[53] X. Duan, J. Yang, H. Gao, J. Ma, L. Jiao, and W. Zheng, "Controllable hydrothermal synthesis of manganese dioxide nanostructures: shape evolution, growth mechanism and electrochemical properties," *CrystEngComm*, vol. 14, no. 12, pp. 4196–4204, 2012.

[54] E. A. Arkhipova, A. S. Ivanov, K. I. Maslakov et al., "Facile hydrothermal synthesis of α-MnO_2 and δ-MnO_2 for pseudocapacitor applications," *Ionics (Kiel)*, vol. 28, no. 7, pp. 3501–3509, 2022.

[55] L. Wang, G. Duan, S.-M. Chen, and X. Liu, "Hydrothermally controlled synthesis of α-MnO_2, γ-MnOOH, and Mn_3O_4 nanomaterials with enhanced electrochemical properties," *Journal of Alloys and Compounds*, vol. 752, pp. 123–132, 2018.

[56] Z. Ren, W. Wu, L. Yu, and Y. Yu, "Hydrothermal synthesis of needle-shaped manganese oxide nanoparticle for superior adsorption of thallium(I): characterization, performance, and mechanism study," *Environmental Science and Pollution Research*, vol. 26, no. 36, pp. 36776–36785, 2019.

[57] G. Cao, L. Su, X. Zhang, and H. Li, "Hydrothermal synthesis and catalytic properties of α- and β-MnO_2 nanorods," *Materials Research Bulletin*, vol. 45, no. 4, pp. 425–428, 2010.

[58] F. Hashemzadeh, M. Mehdi Kashani Motlagh, and A. Maghsoudipour, "A comparative study of hydrothermal and sol–gel methods in the synthesis of MnO_2 nanostructures," *Journal of Sol–Gel Science and Technology*, vol. 51, no. 2, pp. 169–174, 2009.

[59] K. T. Kubra, R. Sharif, B. Patil et al., "Hydrothermal synthesis of neodymium oxide nanoparticles and its nanocomposites with manganese oxide as electrode materials for supercapacitor application," *Journal of Alloys and Compounds*, vol. 815, Article ID 152104, 2020.

[60] Q. Zhang, X. Wu, Q. Zhang et al., "One-step hydrothermal synthesis of MnO_2/graphene composite for electrochemical energy storage," *Journal of Electroanalytical Chemistry*, vol. 837, pp. 108–115, 2019.

[61] D. Shanbhag, K. Bindu, A. R. Aarathy, M. Ramesh, M. Sreejesh, and H. S. Nagaraja, "Hydrothermally synthesized reduced graphene oxide and Sn doped manganese dioxide nanocomposites for supercapacitors and dopamine sensors," *Materials Today Energy*, vol. 4, pp. 66–74, 2017.

[62] B. P. Chhetri, A. Karmakar, and A. Ghosh, "Recent advancements in Ln-ion-based upconverting nanomaterials and their biological applications," *Particle & Particle Systems Characterization*, vol. 36, no. 8, pp. 1–29, 2019.

[63] S. Bach, J. P. Pereira-Ramos, N. Baffier, and R. Messina, "Birnessite manganese dioxide synthesized via a sol–gel process: a new rechargeable cathodic material for lithium batteries," *Electrochimica Acta*, vol. 36, no. 10, pp. 1595–1603, 1991.

[64] M. A. B. Siddique, U. H. Bithi, A. N. Ahmed et al., "Preparation of manganese oxide nanoparticles with enhanced capacitive properties utilizing gel formation method," *ACS Omega*, vol. 7, no. 51, pp. 48007–48017, 2022.

[65] R. Yarbrough, K. Davis, S. Dawood, and H. Rathnayake, "A sol–gel synthesis to prepare size and shape-controlled mesoporous nanostructures of binary (II–VI) metal oxides," *RSC Advances*, vol. 10, no. 24, pp. 14134–14146, 2020.

[66] S. Franger, S. Bach, J. Farcy, J.-P. Pereira-Ramos, and N. Baffier, "Synthesis, structural and electrochemical characterizations of the sol–gel birnessite $MnO_{1.84}{\cdot}0.6H_2O$," *Journal of Power Sources*, vol. 109, no. 2, pp. 262–275, 2002.

[67] S. H. Lee, H. Lee, M. S. Cho, J.-D. Nam, and Y. Lee, "Morphology and composition control of manganese oxide by the pulse reverse electrodeposition technique for high performance supercapacitors," *Journal of Materials Chemistry A*, vol. 1, no. 46, pp. 14606–14611, 2013.

[68] M. Li and H. G. Park, "Improved high-rate performance of a supercapacitor electrode from manganese-oxide-coated vertically aligned carbon nanotubes prepared by a pulsed current electrodeposition method," *Electrochimica Acta*, vol. 296, pp. 676–682, 2019.

[69] M. Nakayama, A. Tanaka, Y. Sato, T. Tonosaki, and K. Ogura, "La050114U.Pdf," pp. 5907–5913, 2005.

[70] J. N. Broughton and M. J. Brett, "Variations in MnO_2 electrodeposition for electrochemical capacitors," *Electrochimica Acta*, vol. 50, no. 24, pp. 4814–4819, 2005.

[71] P. Kanha and P. Saengkwamsawang, "Effect of stirring time on morphology and crystalline features of MnO_2 nanoparticles synthesized by co-precipitation method," *Inorganic and Nano-Metal Chemistry*, vol. 47, no. 8, pp. 1129–1133, 2017.

[72] S. Chen, J. Zhu, Q. Han, Z. Zheng, Y. Yang, and X. Wang, "Shape-controlled synthesis of one-dimensional MnO_2 via a facile quick-precipitation procedure and its electrochemical properties," *Crystal Growth & Design*, vol. 9, no. 10, pp. 4356–4361, 2009.

[73] J. Wang, H. Zhao, J. Song, T. Zhu, and W. Xu, "Structure-activity relationship of manganese oxide catalysts for the catalytic oxidation of (chloro)-VOCs," *Catalysts*, vol. 9, no. 9, Article ID 726, 2019.

[74] J. Shao, F. Lin, Y. Li et al., "Co-precipitation synthesized MnO_x-CeO_2 mixed oxides for no oxidation and enhanced resistance to low concentration of SO_2 by metal addition," *Catalysts*, vol. 9, no. 6, Article ID 519, 2019.

[75] O. A. Bulavchenko, V. P. Konovalova, A. A. Saraev et al., "The catalytic performance of CO oxidation over MnO_x-ZrO_2 catalysts: the role of synthetic routes," *Catalysts*, vol. 13, no. 1, p. 57, 2023.

[76] Y. Shi, P. Ma, L. Qiao, and B. Liu, "Fe–Mn oxide composite activated peroxydisulfate processes for degradation of p-chloroaniline: the effectiveness and the mechanism," *Processes*, vol. 10, no. 11, Article ID 2227, 2022.

[77] J. N. Lacerda, D. F. Franceschini, E. A. Ponzio, L. M. Esteves, R. B. Guimarães, and Y. T. Xing, "Manganese oxide nanofoam prepared by pulsed laser deposition for high performance supercapacitor electrodes," *Materials Chemistry and Physics*, vol. 242, Article ID 122459, 2020.

[78] J. Corrales, J. Acosta, S. Castro et al., "Manganese dioxide nanoparticles prepared by laser ablation as materials with interesting electronic, electrochemical, and disinfecting properties in both colloidal suspensions and deposited on fluorine-doped tin oxide," *Nanomaterials*, vol. 12, no. 22, Article ID 4061, 2022.

[79] H. Xia, Y. Wan, F. Yan, and L. Lu, "Manganese oxide thin films prepared by pulsed laser deposition for thin film microbatteries," *Materials Chemistry and Physics*, vol. 143, no. 2, pp. 720–727, 2014.

[80] S. Isber, E. Majdalani, M. Tabbal, T. Christidis, K. Zahraman, and B. Nsouli, "Study of manganese oxide thin films grown by pulsed laser deposition," *Thin Solid Films*, vol. 517, no. 5, pp. 1592–1595, 2009.

[81] A. Ochirkhuyag, A. Sápi, Á. Szamosvölgyi, G. Kozma, Á. Kukovecz, and Z. Kónya, "One-pot mechanochemical ball milling synthesis of the MnO_x nanostructures as efficient catalysts for CO_2 hydrogenation reactions," *Physical Chemistry Chemical Physics*, vol. 22, no. 25, pp. 13999–14012, 2020.

[82] A. Villanueva, P. de la Presa, J. M. Alonso et al., "Hyperthermia HeLa cell treatment with silica-coated manganese oxide nanoparticles," *The Journal of Physical Chemistry C*, vol. 114, no. 5, pp. 1976–1981, 2010.

[83] M. Pentimalli, M. Bellusci, and F. Padella, "High-energy ball milling as a general tool for nanomaterials synthesis and processing," *Handbook of Mechanical Nanostructuring*, vol. 2, pp. 663–679, 2015.

[84] S. A. Khan, S. Shahid, B. Shahid, U. Fatima, and S. A. Abbasi, "Green synthesis of MnO nanoparticles using abutilon indicum leaf extract for biological, photocatalytic, and adsorption activities," *Biomolecules*, vol. 10, no. 5, Article ID 785, 2020.

[85] M. Souri, V. Hoseinpour, A. Shakeri, and N. Ghaemi, "Optimisation of green synthesis of MnO nanoparticles via utilising response surface methodology," *IET Nanobiotechnology*, vol. 12, no. 6, pp. 822–827, 2018.

[86] H. Lu, X. Zhang, S. A. Khan, W. Li, and L. Wan, "Biogenic synthesis of MnO_2 nanoparticles with leaf extract of viola betonicifolia for enhanced antioxidant, antimicrobial, cytotoxic, and biocompatible applications," *Frontiers in Microbiology*, vol. 12, Article ID 761084, 2021.

[87] K. S. Prasad and A. Patra, "Green synthesis of MnO_2 nanorods using *Phyllanthus amarus* plant extract and their fluorescence studies," *Green Processing and Synthesis*, vol. 6, no. 6, pp. 549–554, 2017.

[88] M. Rahmat, S. Kiran, T. Gulzar et al., "Plant-assisted synthesis and characterization of MnO_2 nanoparticles for removal of crystal violet dye: an environmental remedial approach," *Environmental Science and Pollution Research*, vol. 30, no. 20, pp. 57587–57598, 2023.

[89] R. Munir, K. Ali, S. A. Z. Naqvi, M. A. Maqsood, M. Z. Bashir, and S. Noreen, "Biosynthesis of *Leucaena Leucocephala* leaf mediated ZnO, CuO, MnO_2, and MgO based nano-adsorbents for Reactive Golden Yellow-145 (RY-145) and Direct Red-31 (DR-31) dye removal from textile wastewater to reuse in agricultural purpose," *Separation and Purification Technology*, vol. 306, Article ID 122527, 2023.

[90] T. Khezeli, A. Daneshfar, and F. Kardani, "In-situ functionalization of MnO_2 nanoparticles by natural tea polyphenols: a greener sorbent for dispersive solid-phase extraction of parabens from wastewater and cosmetics," *Microchemical Journal*, vol. 190, Article ID 108751, 2023.

[91] A. Diallo, N. Tandjigora, S. Ndiaye, T. Jan, I. Ahmad, and M. Maaza, "Green synthesis of single phase hausmannite Mn_3O_4 nanoparticles via *Aspalathus linearis* natural extract," *SN Applied Sciences*, vol. 3, no. 5, pp. 1–11, 2021.

[92] T. V. Tran, D. T. C. Nguyen, P. S. Kumar, A. T. M. Din, A. S. Qazaq, and D.-V. N. Vo, "Green synthesis of Mn_3O_4 nanoparticles using *Costus woodsonii* flowers extract for

effective removal of malachite green dye," *Environmental Research*, vol. 214, Article ID 113925, 2022.

[93] A. S. Prasad, "Green synthesis of nanocrystalline manganese (II, III) oxide," *Materials Science in Semiconductor Processing*, vol. 71, pp. 342–347, 2017.

[94] A. Thanigaivel, S. Senthil-Nathan, P. Vasantha-Srinivasan et al., "Chemicals isolated from *Justicia adhatoda* Linn reduce fitness of the mosquito, *Aedes aegypti* L." *Archives of Insect Biochemistry and Physiology*, vol. 94, no. 4, pp. 1–11, 2017.

[95] J. K. Sharma, P. Srivastava, S. Ameen, M. S. Akhtar, G. Singh, and S. Yadava, "Azadirachta indica plant-assisted green synthesis of Mn_3O_4 nanoparticles: excellent thermal catalytic performance and chemical sensing behavior," *Journal of Colloid and Interface Science*, vol. 472, pp. 220–228, 2016.

[96] G. N. Sreekala, F. Abdullakutty, and B. Beena, "Green synthesis, characterization, and photo catalytic degradation efficiency of trimanganese tetroxide nanoparticle," *International Journal of Nano Dimension*, vol. 10, no. 4, pp. 400–409, 2019.

[97] H. S. Sumantha, S. Rajagopal, M. Shashank et al., "Green synthesis and characterization of Mn_3O_4 nanoparticles for photocatalytic and supercapacitors," *Ionics*, vol. 29, no. 2, pp. 733–749, 2023.

[98] P. Premakumari, H. K. E. Latha, and G. Nagaraju, "Green synthesis of dimanganese trioxide nanoparticles using tamarind seed powder: effect of tamarind seed powder concentration on the structural, electrical and electrochemical properties of dimanganese trioxide nanoparticles," *Materials Today: Proceedings*, vol. 49 Part 3, pp. 554–558, 2021.

[99] M. Souri, V. Hoseinpour, N. Ghaemi, and A. Shakeri, "Procedure optimization for green synthesis of manganese dioxide nanoparticles by *Yucca gloriosa* leaf extract," *International Nano Letters*, vol. 9, no. 1, pp. 73–81, 2019.

[100] A. Sinha, V. N. Singh, B. R. Mehta, and S. K. Khare, "Synthesis and characterization of monodispersed orthorhombic manganese oxide nanoparticles produced by *Bacillus* sp. cells simultaneous to its bioremediation," *Journal of Hazardous Materials*, vol. 192, no. 2, pp. 620–627, 2011.

[101] B. Hosseinkhani and G. Emtiazi, "Synthesis and characterization of a novel extracellular biogenic manganese oxide (bixbyite-like Mn_2O_3) nanoparticle by isolated *Acinetobacter* sp." *Current Microbiology*, vol. 63, pp. 300–305, 2011.

[102] B. K. Salunke, S. S. Sawant, S.-I. Lee, and B. S. Kim, "Comparative study of MnO_2 nanoparticle synthesis by marine bacterium *Saccharophagus degradans* and yeast *Saccharomyces cerevisiae*," *Applied Microbiology and Biotechnology*, vol. 99, no. 13, pp. 5419–5427, 2015.

[103] Y. Shi, M. Zhang, D. Yang, and J. Li, "Study on preparation of high performance manganese dioxide supercapacitor by cyclic voltammetry," *Ionics*, vol. 27, no. 10, pp. 4521–4529, 2021.

[104] W. Sheng, W. Wei, J. Li et al., "Amine-functionalized magnetic mesoporous silica nanoparticles for DNA separation," *Applied Surface Science*, vol. 387, pp. 1116–1124, 2016.

[105] S. Sivakumar and L. Nelson Prabu, "Synthesis and characterization of α-MnO_2 nanoparticles for supercapacitor application," *Materials Today: Proceedings*, vol. 47, pp. 52–55, 2021.

[106] S. A. Jacob, R. Ragu, M. M. Jaculine, A. Daisy, and S. J. Das, "Exploring the consequences of lanthanum incorporation on micro-structural, nanoscale morphological and magnetic traits on manganese dioxide nanoparticles," *Journal of Materials Science: Materials in Electronics*, vol. 33, no. 9, pp. 6856–6871, 2022.

[107] S.-Y. Xu, L.-Y. Lin, and H.-Y. Lin, "Novel flexible solid-state pseudo-parallel pseudocapacitor with manganese oxide active material synthesized using electrodeposition," *Journal of Alloys and Compounds*, vol. 843, Article ID 156017, 2020.

[108] M. Cetina-Dorantes, F. I. Lizama-Tzec, M. A. Estrella-Gutiérrez, D. M. Herrera-Zamora, O. Arés-Muzio, and G. Oskam, "Electrodeposition of cobalt-manganese oxide selective coatings for solar-thermal applications," *Electrochimica Acta*, vol. 391, Article ID 138906, 2021.

[109] P. Jain, S. Bhagat, L. Tunki et al., "Serotonin–stearic acid bioconjugate-coated completely biodegradable Mn_3O_4 nanocuboids for hepatocellular carcinoma targeting," *ACS Applied Materials & Interfaces*, vol. 12, no. 9, pp. 10170–10182, 2020.

[110] G. Anguraj, R. A. Kumar, C. Inmozhi et al., "MnO_2 doped with Ag nanoparticles and their applications in antimicrobial and photocatalytic reactions," *Catalysts*, vol. 13, no. 2, Article ID 397, 2023.

[111] A. Feng, T. Hou, Z. Jia, and G. Wu, "Synthesis of a hierarchical carbon fiber@cobalt ferrite@manganese dioxide composite and its application as a microwave absorber," *RSC Advances*, vol. 10, no. 18, pp. 10510–10518, 2020.

[112] R. Yuan, H. Li, X. Zhang, H. Zhu, J. Zhao, and R. Chen, "Facile one-pot solvothermal synthesis of bifunctional chrysanthemum-like cobalt-manganese oxides for supercapacitor and degradation of pollutants," *Journal of Energy Storage*, vol. 29, Article ID 101300, 2020.

[113] K. Gupta, S. Bhattacharya, D. Chattopadhyay et al., "Ceria associated manganese oxide nanoparticles: synthesis, characterization and arsenic(V) sorption behavior," *Chemical Engineering Journal*, vol. 172, no. 1, pp. 219–229, 2011.

[114] S. A. Moon, B. K. Salunke, B. Alkotaini, E. Sathiyamoorthi, and B. S. Kim, "Biological synthesis of manganese dioxide nanoparticles by *Kalopanax pictus* plant extract," *IET Nanobiotechnology*, vol. 9, no. 4, pp. 220–225, 2015.

[115] S. Salatin, J. Barar, M. Barzegar-Jalali, K. Adibkia, F. Kiafar, and M. Jelvehgari, "Development of a nanoprecipitation method for the entrapment of a very water soluble drug into Eudragit RL nanoparticles," *Research in Pharmaceutical Sciences*, vol. 12, no. 1, pp. 1–14, 2017.

[116] J. Dolai, K. Mandal, and N. R. Jana, "Nanoparticle size effects in biomedical applications," *ACS Applied Nano Materials*, vol. 4, no. 7, pp. 6471–6496, 2021.

[117] S. K. Nune, P. Gunda, P. K. Thallapally, Y.-Y. Lin, M. Laird Forrest, and C. J. Berkland, "Nanoparticles for biomedical imaging," *Expert Opinion on Drug Delivery*, vol. 6, no. 11, pp. 1175–1194, 2009.

[118] M. Adabi, M. Naghibzadeh, M. Adabi et al., "Biocompatibility and nanostructured materials: applications in nanomedicine," *Artificial Cells, Nanomedicine, and Biotechnology*, vol. 45, no. 4, pp. 833–842, 2017.

[119] Z. Chen, Z. Jiao, D. Pan et al., "Recent advances in manganese oxide nanocrystals: fabrication, characterization, and microstructure," *Chemical Reviews*, vol. 112, no. 7, pp. 3833–3855, 2012.

[120] F. C. Simeone and A. L. Costa, "Assessment of cytotoxicity of metal oxide nanoparticles on the basis of fundamental physical–chemical parameters: a robust approach to grouping," *Environmental Science: Nano*, vol. 6, no. 10, pp. 3102–3112, 2019.

[121] S. Haque, S. Tripathy, and C. R. Patra, "Manganese-based advanced nanoparticles for biomedical applications: future

opportunity and challenges," *Nanoscale*, vol. 13, no. 39, pp. 16405–16426, 2021.

[122] R. G. D. Andrade, D. Ferreira, S. R. S. Veloso et al., "Synthesis and cytotoxicity assessment of citrate-coated calcium and manganese ferrite nanoparticles for magnetic hyperthermia," *Pharmaceutics*, vol. 14, no. 12, Article ID 2694, 2022.

[123] E. Silveira-Alves Jr, F. C. Bezerra, R. A. Guerra et al., "Coupling of cationic porphyrins on manganese ferrite nanoparticles: a potential multifunctional nanostructure for theranostics applications," *Journal of Photochemistry and Photobiology A: Chemistry*, vol. 438, Article ID 114551, 2023.

[124] M. Anithkumar, A. Rajan S, A. Khan et al., "Glucose oxidase-loaded $MnFe_2O_4$ nanoparticles for hyperthermia and cancer starvation therapy," *ACS Applied Nano Materials*, vol. 6, no. 4, pp. 2605–2614, 2023.

[125] R. Joshi, S. B. Shelar, M. Srivastava, B. P. Singh, L. Goel, and R. S. Ningthoujam, "Development of Core@Shell γ-Fe_2O_3 @Mn_x O_y @SiO_2 nanoparticles for hyperthermia, targeting, and imaging applications," *ACS Applied Bio Materials*, vol. 5, no. 11, pp. 5386–5393, 2022.

[126] R. Gupta and D. Sharma, "Manganese-doped magnetic nanoclusters for hyperthermia and photothermal glioblastoma therapy," *ACS Applied Nano Materials*, vol. 3, no. 2, pp. 2026–2037, 2020.

[127] S. S. Phalake, M. S. Lad, K. V. Kadam, S. A. M. Tofail, N. D. Thorat, and V. M. Khot, "Application of $Mn_xFe_{1-x}Fe_2O_4(x=0-1)$ nanoparticles in magnetic fluid hyperthermia: correlation with cation distribution and magnetostructural properties," *ACS Omega*, vol. 48, pp. 44187–44198, 2022.

[128] K. Shah, A. Bhardwaj, D. Bhadla, K. Parekh, and N. Jain, "Cytotoxicity and uptake analysis of Mn–Zn ferrite-based temperature-sensitive ferrofluid on cervical and bone cancer cells," *Journal of Magnetism and Magnetic Materials*, vol. 589, Article ID 171534, 2024.

[129] A. Singh, P. Kumar, S. Pathak et al., "Tailored nanoparticles for magnetic hyperthermia: highly stable aqueous dispersion of Mn-substituted magnetite superparamagnetic nanoparticles by double surfactant coating for improved heating efficiency," *Journal of Alloys and Compounds*, vol. 976, Article ID 172999, 2024.

[130] S. Del Sol Fernández, O. F. Odio, P. M. Crespo et al., "Tunable control of the structural features and related physical properties of $Mn_xFe_{3-x}O_4$ nanoparticles : implication on their heating performance by magnetic hyperthermia," *The Journal of Physical Chemistry C*, vol. 126, no. 24, pp. 10110–10128, 2022.

[131] S. Nasrin, F.-U.-Z. Chowdhury, and S. M. Hoque, "Study of hyperthermia temperature of manganese-substituted cobalt nano ferrites prepared by chemical co-precipitation method for biomedical application," *Journal of Magnetism and Magnetic Materials*, vol. 479, pp. 126–134, 2019.

[132] S. P. Gajare, P. A. Bansode, P. V. Patil et al., "Anticancer, antibacterial and hyperthermia studies of a caffeine-based *N*-heterocyclic carbene silver complex anchored on magnetic nanoparticles," *ChemistrySelect*, vol. 6, no. 9, pp. 1958–1968, 2021.

[133] M. Lickmichand, C. S. Shaji, N. Valarmathi et al., "In vitro biocompatibility and hyperthermia studies on synthesized cobalt ferrite nanoparticles encapsulated with polyethylene glycol for biomedical applications," *Materials Today: Proceedings*, vol. 15, pp. 252–261, 2019.

[134] J. Zeng, L. Jing, Y. Hou et al., "Anchoring group effects of surface ligands on magnetic properties of Fe_3O_4 nanoparticles: towards high performance MRI contrast agents," *Advanced Materials*, vol. 26, no. 17, pp. 2694–2698, 2014.

[135] S. Arsalani, E. J. Guidelli, M. A. Silveira et al., "Magnetic Fe_3O_4 nanoparticles coated by natural rubber latex as MRI contrast agent," *Journal of Magnetism and Magnetic Materials*, vol. 475, pp. 458–464, 2019.

[136] S. Hong, Y. Chang, and I. Rhee, "Chitosan-coated ferrite (Fe_3O_4) nanoparticles as a T_2 contrast agent for magnetic resonance imaging," *Journal of the Korean Physical Society*, vol. 56, no. 3, pp. 868–873, 2010.

[137] S. Xu, J. Wang, Y. Wei et al., "*In situ* one-pot synthesis of Fe_2O_3@BSA core-shell nanoparticles as enhanced T_1-weighted magnetic resonance imagine contrast agents," *ACS Applied Materials & Interfaces*, vol. 12, no. 51, pp. 56701–56711, 2020.

[138] E. Taboada, R. Solanas, E. Rodríguez, R. Weissleder, and A. Roig, "Supercritical-fluid-assisted one-pot synthesis of biocompatible core (γ-Fe_2O_3)/Shell(SiO_2) nanoparticles as high relaxivity T_2-contrast agents for magnetic resonance imaging," *Advanced Functional Materials*, vol. 19, no. 14, pp. 2319–2324, 2009.

[139] X. He, F. Liu, L. Liu, T. Duan, H. Zhang, and Z. Wang, "Lectin-conjugated Fe_2O_3 @Au Core@Shell nanoparticles as dual mode contrast agents for *in vivo* detection of tumor," *Molecular Pharmaceutics*, vol. 11, no. 3, pp. 738–745, 2014.

[140] O. Bomatí-Miguel, M. P. Morales, P. Tartaj et al., "Fe-based nanoparticulate metallic alloys as contrast agents for magnetic resonance imaging," *Biomaterials*, vol. 26, no. 28, pp. 5695–5703, 2005.

[141] A. P. Koretsky and A. C. Silva, "Manganese-enhanced magnetic resonance imaging (MEMRI)," *NMR in Biomedicine*, vol. 17, no. 8, pp. 527–531, 2004.

[142] C. A. Massaad and R. G. Pautler, "Manganese-enhanced magnetic resonance imaging (MEMRI)," in *Magnetic Resonance Neuroimaging*, M. Modo and J. Bulte, Eds., vol. 711 of *Methods in Molecular Biology*, pp. 145–174, Humana Press, 2011.

[143] T. Kim, E.-J. Cho, Y. Chae et al., "Urchin-shaped manganese oxide nanoparticles as pH-responsive activatable T_1 contrast agents for magnetic resonance imaging," *Angewandte Chemie*, vol. 123, no. 45, pp. 10777–10781, 2011.

[144] L. B. Mithal, P. S. Patel, D. Mithal, H. L. Palac, and M. N. Rozenfeld, "Use of gadolinium-based magnetic resonance imaging contrast agents and awareness of brain gadolinium deposition among pediatric providers in North America," *Pediatric Radiology*, vol. 47, no. 6, pp. 657–664, 2017.

[145] M. S. Usman, M. Z. Hussein, S. Fakurazi, and F. F. Ahmad Saad, "Gadolinium-based layered double hydroxide and graphene oxide nano-carriers for magnetic resonance imaging and drug delivery," *Chemistry Central Journal*, vol. 11, no. 1, Article ID 47, 2017.

[146] C. Olchowy, K. Cebulski, M. Łasecki et al., "The presence of the gadolinium-based contrast agent depositions in the brain and symptoms of gadolinium neurotoxicity—a systematic review," *PLOS ONE*, vol. 12, no. 2, Article ID e0171704, 2017.

[147] H. J. Gerritsen and E. S. Sabisky, "Paramagnetic resonance of trivalent manganese in rutile (TiO_2)," *Physical Review*, vol. 132, no. 4, pp. 1507–1512, 1963.

[148] B. Bleaney and D. J. E. Ingram, "The paramagnetic resonance spectra of two salts of manganese," *Proceedings*

of the Royal Society of London. Series A. Mathematical and Physical Sciences, vol. 205, no. 1082, pp. 336–356, 1951.

[149] M. Blume and R. Orbach, "Spin-lattice relaxation of *S*-state ions: Mn^{2+} in a cubic environment," *Physical Review*, vol. 127, no. 5, pp. 1587–1592, 1962.

[150] K. Nelson, J. Golnick, T. Korn, and C. Angle, "Manganese encephalopathy: utility of early magnetic resonance imaging," *Occupational and Environmental Medicine*, vol. 50, no. 6, pp. 510–513, 1993.

[151] E. M. Gale, I. P. Atanasova, F. Blasi, I. Ay, and P. Caravan, "A manganese alternative to gadolinium for MRI contrast," *Journal of the American Chemical Society*, vol. 137, no. 49, pp. 15548–15557, 2015.

[152] C. Henoumont, M. Devreux, and S. Laurent, "Mn-based MRI contrast agents: an overview," *Molecules*, vol. 28, no. 21, Article ID 7275, 2023.

[153] A. B. Bowman, G. F. Kwakye, E. Herrero Hernández, and M. Aschner, "Role of manganese in neurodegenerative diseases," *Journal of Trace Elements in Medicine and Biology*, vol. 25, no. 4, pp. 191–203, 2011.

[154] I. Aoki, S. Naruse, and C. Tanaka, "Manganese-enhanced magnetic resonance imaging (MEMRI) of brain activity and applications to early detection of brain ischemia," *NMR in Biomedicine*, vol. 17, no. 8, pp. 569–580, 2004.

[155] Z. Mo, M. Qiu, K. Zhao et al., "Multifunctional phototheranostic nanoplatform based on polydopamine-manganese dioxide-IR780 iodide for effective magnetic resonance imaging-guided synergistic photodynamic/photothermal therapy," *Journal of Colloid and Interface Science*, vol. 611, pp. 193–204, 2022.

[156] S. V. Lopes, P. Walczak, M. Janowski, R. L. Reis, J. Silva-Correia, and J. M. Oliveira, "Cytocompatible manganese dioxide-based hydrogel nanoreactors for MRI imaging," *Biomaterials Advances*, vol. 134, Article ID 112575, 2022.

[157] Y. Hou, Z. Tang, J. Farheen et al., "Ovalbumin-loaded paramagnetic nano-triangles for enhanced dendritic cell stimulation, T1-MR imaging, and antitumor immunity," *Journal of Materials Science & Technology*, vol. 148, pp. 123–137, 2023.

[158] J. Cai, S. Jiang, J. Liao et al., "Manganese-doped biostimulatory nanoneedle for MRI-visual bispecific antibody gene delivery and immunosuppression reversal as a cancer immunotherapy strategy," *Chemical Engineering Journal*, vol. 462, Article ID 142242, 2023.

[159] M. F. Casula, E. Conca, I. Bakaimi et al., "Manganese doped-iron oxide nanoparticle clusters and their potential as agents for magnetic resonance imaging and hyperthermia," *Physical Chemistry Chemical Physics*, vol. 18, no. 25, pp. 16848–16855, 2016.

[160] S. Xiao, X. Yu, L. Zhang et al., "Synthesis of peg-coated, ultrasmall, manganese-doped iron oxide nanoparticles with high relaxivity for T_1/T_2 dual-contrast magnetic resonance imaging," *International Journal of Nanomedicine*, vol. 14, pp. 8499–8507, 2019.

[161] R. Zhou, S. Sun, C. Li, L. Wu, X. Hou, and P. Wu, "Enriching Mn-doped ZnSe quantum dots onto mesoporous silica nanoparticles for enhanced fluorescence/magnetic resonance imaging dual-modal bio-imaging," *ACS Applied Materials & Interfaces*, vol. 10, no. 40, pp. 34060–34067, 2018.

[162] Y. Zhao, Y. Pan, K. Zou et al., "Biomimetic manganese-based theranostic nanoplatform for cancer multimodal imaging and twofold immunotherapy," *Bioactive Materials*, vol. 19, pp. 237–250, 2023.

[163] Y. Shi, Y. Shi, Z. Wang et al., "Glucose-responsive mesoporous prussian blue nanoprobes coated with ultrasmall gold and manganese dioxide for magnetic resonance imaging and enhanced antitumor therapy," *Chemical Engineering Journal*, vol. 453, Article ID 139885, 2023.

[164] S. Kunuku, B.-R. Lin, C.-H. Chen et al., "Nanodiamonds doped with manganese for applications in magnetic resonance imaging," *ACS Omega*, vol. 8, no. 4, pp. 4398–4409, 2023.

[165] J. Shin, R. M. Anisur, M. K. Ko, G. H. Im, J. H. Lee, and I. S. Lee, "Hollow manganese oxide nanoparticles as multifunctional agents for magnetic resonance imaging and drug delivery," *Angewandte Chemie International Edition*, vol. 48, no. 2, pp. 321–324, 2009.

[166] W. Xu, X. Qing, S. Liu, D. Yang, X. Dong, and Y. Zhang, "Hollow mesoporous manganese oxides: application in cancer diagnosis and therapy," *Small*, vol. 18, no. 15, Article ID 2106511, 2022.

[167] D. Zhu, X.-H. Zhu, S.-Z. Ren, Y.-D. Lu, and H.-L. Zhu, "Manganese dioxide (MnO_2) based nanomaterials for cancer therapies and theranostics," *Journal of Drug Targeting*, vol. 29, no. 9, pp. 911–924, 2021.

[168] Z. Sobańska, J. Roszak, K. Kowalczyk, and M. Stępnik, "Applications and biological activity of nanoparticles of manganese and manganese oxides in in vitro and in vivo models," *Nanomaterials*, vol. 11, no. 5, Article ID 1084, 2021.

[169] S. Vaidya, A. Kar, A. Patra, and A. K. Ganguli, "Core–shell (CS) nanostructures and their application based on magnetic and optical properties," *Reviews in Nanoscience and Nanotechnology*, vol. 2, no. 2, pp. 106–126, 2013.

[170] X. Liu and P. Rong, "Recent advances of manganese-based hybrid nanomaterials for cancer precision medicine," *Frontiers in Oncology*, vol. 11, Article ID 707618, 2021.

[171] P. Yadav, A. Bhaduri, and A. Thakur, "Manganese oxide nanoparticles: an insight into structure, synthesis and applications," *ChemBioEng Reviews*, vol. 10, no. 4, pp. 510–528, 2023.

[172] S. Dawadi, A. Gupta, M. Khatri, B. Budhathoki, G. Lamichhane, and N. Parajuli, "Manganese dioxide nanoparticles: synthesis, application and challenges," *Bulletin of Materials Science*, vol. 43, no. 1, Article ID 277, 2020.

[173] J. Chen, H. Meng, Y. Tian et al., "Recent advances in functionalized MnO_2 nanosheets for biosensing and biomedicine applications," *Nanoscale Horizons*, vol. 4, no. 2, pp. 321–338, 2019.

[174] Z. Zhang and Y. Ji, "Nanostructured manganese dioxide for anticancer applications: preparation, diagnosis, and therapy," *Nanoscale*, vol. 12, no. 35, pp. 17982–18003, 2020.

[175] E. Yasun, S. Gandhi, S. Choudhury et al., "Hollow micro- and nanostructures for therapeutic and imaging applications," *Journal of Drug Delivery Science and Technology*, vol. 60, Article ID 102094, 2020.

[176] J. Wen, K. Yang, and S. Sun, "MnO_2-based nanosystems for cancer therapy," *Chemical Communications*, vol. 56, no. 52, pp. 7065–7079, 2020.

[177] G. Yang, J. Ji, and Z. Liu, "Multifunctional MnO_2 nanoparticles for tumor microenvironment modulation and cancer therapy," *WIREs Nanomedicine and Nanobiotechnology*, vol. 13, no. 6, Article ID e1720, 2021.

[178] X. Xu, J. Duan, Y. Liu et al., "Multi-stimuli responsive hollow MnO_2-based drug delivery system for magnetic resonance

imaging and combined chemo-chemodynamic cancer therapy," *Acta Biomaterialia*, vol. 126, pp. 445–462, 2021.

[179] J. Du, J. Sun, X. Liu et al., "Preparation of C6 cell membrane-coated doxorubicin conjugated manganese dioxide nanoparticles and its targeted therapy application in glioma," *European Journal of Pharmaceutical Sciences*, vol. 180, Article ID 106338, 2023.

[180] D. He, X. He, K. Wang et al., "Redox-responsive degradable honeycomb manganese oxide nanostructures as effective nanocarriers for intracellular glutathione-triggered drug release," *Chemical Communications*, vol. 51, no. 4, pp. 776–779, 2015.

[181] C. Tan, J. Wu, and Z. Wen, "Doxorubicin-loaded MnO_2@Zeolitic imidazolate framework-8 nanoparticles as a chemophotothermal system for lung cancer therapy," *ACS Omega*, vol. 6, no. 20, pp. 12977–12983, 2021.

[182] H.-L. Zhang, Y. Wang, Q. Tang, B. Ren, S.-P. Yang, and J.-G. Liu, "A mesoporous MnO_2-based nanoplatform with near infrared light-controlled nitric oxide delivery and tumor microenvironment modulation for enhanced antitumor therapy," *Journal of Inorganic Biochemistry*, vol. 241, Article ID 112133, 2023.

[183] Y. Zheng, H. Zhang, Y. Hu, L. Bai, and J. Xue, "MnO nanoparticles with potential application in magnetic resonance imaging and drug delivery for myocardial infarction," *International Journal of Nanomedicine*, vol. 13, pp. 6177–6188, 2018.

[184] P. Jain, K. Patel, A. K. Jangid et al., "Biotinylated Mn_3O_4 nanocuboids for targeted delivery of gemcitabine hydrochloride to breast cancer and MRI applications," *International Journal of Pharmaceutics*, vol. 606, Article ID 120895, 2021.

[185] M. Zhou, X. Wang, S. Lin et al., "Multifunctional STING-Activating Mn_3O_4 @Au-dsDNA/DOX nanoparticle for antitumor immunotherapy," *Advanced Healthcare Materials*, vol. 9, no. 13, Article ID 2000064, 2020.

[186] M. Arjama, S. Mehnath, and M. Jeyaraj, "Self-assembled hydrogel nanocube for stimuli responsive drug delivery and tumor ablation by phototherapy against breast cancer," *International Journal of Biological Macromolecules*, vol. 213, pp. 435–446, 2022.

[187] J. Li, X. Peng, J. Tao et al., "Facile synthesis of triple-hybrid organosilica/manganese dioxide hybrid nanoparticles for glutathione-adaptive shape-morphing and improving cellular drug delivery," *Journal of the Taiwan Institute of Chemical Engineers*, vol. 142, Article ID 104669, 2023.

[188] X. Zhao, S. He, B. Li et al., "DUCNP@Mn–MOF/FOE as a highly selective and bioavailable drug delivery system for synergistic combination cancer therapy," *Nano Letters*, vol. 23, no. 3, pp. 863–871, 2023.

[189] V. Sabaghi, P. Rashidi-Ranjbar, F. Davar, and E. Sharif-Paghaleh, "Development of multifunctional MnO_2-based nanoplatforms for hypoxia modulation/*T*1-weighted MRI/optical biosensing and targeted drug delivery," *Journal of Drug Delivery Science and Technology*, vol. 91, Article ID 105190, 2024.

[190] Y. Miao, X. Zhou, J. Bai, W. Zhao, and X. Zhao, "Hollow polydopamine spheres with removable manganese oxide nanoparticle caps for tumor microenvironment-responsive drug delivery," *Chemical Engineering Journal*, vol. 430, Article ID 133089, 2022.

[191] W. Wang, X. Chen, J. Li, Q. Jin, H. J. Jin, and X. Li, "Hollow MnO_2 nanoparticles loaded with functional genes as nanovaccines for synergistic cancer therapy," *ACS Applied Nano Materials*, vol. 5, no. 8, pp. 10537–10547, 2022.

[192] S. Jiang, X. Li, F. Zhang et al., "Manganese dioxide-based nanocarrier delivers paclitaxel to enhance chemotherapy against orthotopic glioma through hypoxia relief," *Small Methods*, vol. 6, no. 7, Article ID 2101531, 2022.

[193] Z. Wang, C. Wu, J. Liu et al., "Aptamer-mediated hollow MnO_2 for targeting the delivery of sorafenib," *Drug Delivery*, vol. 30, no. 1, pp. 28–39, 2023.

[194] M. Samiei Foroushani, A. Zahmatkeshan, H. Arkaban, R. Karimi Shervedani, and A. Kefayat, "A drug delivery system based on nanocomposites constructed from metal-organic frameworks and Mn_3O_4 nanoparticles: preparation and physicochemical characterization for BT-474 and MCF-7 cancer cells," *Colloids and Surfaces B: Biointerfaces*, vol. 202, Article ID 111712, 2021.

[195] H. Arkaban, R. Karimi Shervedani, F. Yaghoobi, A. Kefayat, and F. Ghahremani, "Imaging and therapeutic capabilities of the AuNPs@$MnCO_3$/Mn_3O_4, coated with PAA and integrated with folic acid, doxorubicin and propidium iodide for murine breast cancer," *Journal of Drug Delivery Science and Technology*, vol. 67, Article ID 102818, 2022.

[196] H. Wang, D. H. Bremner, K. Wu et al., "Platelet membrane biomimetic bufalin-loaded hollow MnO_2 nanoparticles for MRI-guided chemo-chemodynamic combined therapy of cancer," *Chemical Engineering Journal*, vol. 382, Article ID 122848, 2020.

[197] Z. Deng, G. Qiao, L. Ma, Q. Zhang, P. Zhang, and D. Cui, "Photosensitizer-functionalized Mn@Co magnetic nanoparticles for MRI/NIR-mediated photothermal therapy of gastric cancer," *ACS Applied Nano Materials*, vol. 4, no. 12, pp. 13523–13533, 2021.

[198] H. H. Farhan and A. M. Mohammed, "Biosynthesis and evaluation of MnO_2 nanoparticles as anti-oxidant and anti-diabetic agents," *Results in Chemistry*, vol. 7, Article ID 101266, 2024.

[199] S. Pardhiya, E. Priyadarshini, and P. Rajamani, "In vitro antioxidant activity of synthesized BSA conjugated manganese dioxide nanoparticles," *SN Applied Sciences*, vol. 2, no. 9, Article ID 1597, 2020.

[200] Y. Zhang, L. Chen, R. Sun et al., "Multienzymatic antioxidant activity of manganese-based nanoparticles for protection against oxidative cell damage," *ACS Biomaterials Science & Engineering*, vol. 8, no. 2, pp. 638–648, 2022.

[201] R. K. Kunkalekar, M. M. Naik, S. K. Dubey, and A. V. Salker, "Antibacterial activity of silver-doped manganese dioxide nanoparticles on multidrug-resistant bacteria," *Journal of Chemical Technology & Biotechnology*, vol. 88, no. 5, pp. 873–877, 2013.

[202] Z. Zhang and Y. Ji, "Mesoporous manganese dioxide coated gold nanorods as a multiresponsive nanoplatform for drug delivery," *Industrial & Engineering Chemistry Research*, vol. 58, no. 8, pp. 2991–2999, 2019.

[203] A. Mahmood, T. Munir, A. Rasul, A. A. Ghfar, and S. Mumtaz, "Polyethylene glycol and chitosan functionalized manganese oxide nanoparticles for antimicrobial and anticancer activities," *Journal of Colloid and Interface Science*, vol. 648, pp. 907–915, 2023.

[204] X. Qian, X. Han, L. Yu, T. Xu, and Y. Chen, "Manganese-based functional nanoplatforms: nanosynthetic construction, physiochemical property, and theranostic applicability," *Advanced Functional Materials*, vol. 30, no. 3, Article ID 1907066, 2020.

[205] K. H. Bae, K. Lee, C. Kim, and T. G. Park, "Surface functionalized hollow manganese oxide nanoparticles for cancer targeted siRNA delivery and magnetic resonance imaging," *Biomaterials*, vol. 32, no. 1, pp. 176–184, 2011.

[206] L. Liu, C. Wang, Y. Li et al., "Manganese dioxide nanozyme for reactive oxygen therapy of bacterial infection and wound healing," *Biomaterials Science*, vol. 9, no. 17, pp. 5965–5976, 2021.

[207] J. Ruan and H. Qian, "Recent development on controlled synthesis of Mn-based nanostructures for bioimaging and cancer therapy," *Advanced Therapeutics*, vol. 4, no. 5, Article ID 2100018, 2021.

[208] G. Ijaz Dar, M. Z. Iqbal, O. U. Akakuru, C. Yao, G. Awiaz, and A. Wu, "Facile synthesis of Au@Mn_3O_4 magneto-plasmonic nanoflowers for T_1-weighted magnetic resonance imaging and photothermal therapy of cancer," *Journal of Materials Chemistry B*, vol. 8, no. 36, pp. 8356–8367, 2020.

[209] V. P. Tolstoy, L. B. Gulina, A. A. Golubeva et al., "Thin layers formed by the oriented 2D nanocrystals of birnessite-type manganese oxide as a new electrochemical platform for ultrasensitive nonenzymatic hydrogen peroxide detection," *Journal of Solid State Electrochemistry*, vol. 23, no. 2, pp. 573–582, 2019.

[210] N. Chauhan, S. Balayan, and U. Jain, "Sensitive biosensing of neurotransmitter: 2D material wrapped nanotubes and MnO_2 composites for the detection of acetylcholine," *Synthetic Metals*, vol. 263, Article ID 116354, 2020.

[211] X. Gao, H. Zhang, L. Liu, M. Jia, X. Li, and J. Li, "Nano-biosensor based on manganese dioxide nanosheets and carbon dots for dual-mode determination of *Staphylococcus aureus*," *Food Chemistry*, vol. 432, Article ID 137144, 2024.